Alma Mater Studiorum · Università di Bologna

Scuola di Scienze
Dipartimento di Fisica e Astronomia
Corso di Laurea Magistrale in Fisica del Sistema Terra

THE ROLE OF PASSIVE MARGINS IN THE CONTINENTAL COLLISION DYNAMICS

Relatore:
Prof. Andrea Morelli

Correlatore:
Dott. Valentina Magni

Presentata da:
Valeria Turino

Sessione 3
Anno Accademico 2018/2019

Contents

Abstract

La transizione tra litosfera continentale ed oceanica nei margini passivi può avere caratteristiche diverse che dipendono principalmente dall'evoluzione tettonica regionale durante la loro formazione. I margini passivi creati dal processo di *rifiting* sono caratterizzati da una zona tra continente e oceano costituita da litosfera continentale assottigliata a seguito dell'estensione. La velocità e la durata del processo di rifting influenza le dimensioni e la geometria del margine passivo. Inoltre, i margini passivi denominati *magma rich* sono associati ad una elevata produzione di magma derivante dalla fusione del mantello e alla conseguente messa in posto di rocce mafiche intrusive ed effusive, mentre questo non avviene nel caso di margini *magma poor*. Tutte queste differenze fanno sì che la geometria e, soprattuto, la reologia dei margini passivi siano molto varie.

In questo progetto ho studiato come i diversi tipi di margini passivi, una volta arrivati alla zona di cerniera, influenzino la dinamica della subduzione e collisione continentale. In particolare, i fenomeni che sono stati studiati sono la rottura dello slab in profondità e l'accrezione di crosta continentale alla placca sovrascorrente. Questi processi, che sono solo alcuni degli scenari che possono avvenire in zone di collisione continentale, sono influenzati dalle caratteristiche del margine passivo.

Per questo studio, ho sviluppato dei modelli bidimensionali di subduzione con geometrie, reologie e composizioni dei margini passivi diverse, utilizzando un codice di modellazione numerica ad elementi finiti (Citcom) adatto a modellare problemi di convezione mantellica. Lo scopo di questi modelli è quello di avere una migliore comprensione del processo di subduzione e capire ed interpretare la geologia delle zone di collisione continentale.

I risultati mostrano che la presenza di margini passivi ha un impatto importante sul processo di subduzione. Si vede, infatti, che la variazione di profondità del break-off dello slab varia su 300 km, mentre quella del tempo relativo al break-off è di 50 Myr. I modelli che descrivono i margini magma poor, inoltre, sono consistenti con osservazioni geologiche che mostrano che parte del margine viene trasferito sulla placca sovrascorrente. Quelli che modellano i margini magma rich, invece, mostrano che il break-off avviene al di sopra del margine, e questo è in linea con le osservazioni che mostrano che è raro osservare margini di questo tipo in natura.

Chapter 1

Introduction

Ocean-continent boundaries at passive margins are extremely diverse and might be important regions in which the deformation is accommodated during continental collision. However, their different architecture is often neglected in numerical studies of subduction and continental collision dynamics. The aim of this work is to understand how the presence of different types of passive margins affects subduction dynamics when it comes to continental collision. In particular, I focused on changes in the geometry, density, and rheology of the margin to better simulate the characteristics of real margins we can find on our planet. This study will allow us to understand if neglecting the presence of these structures is justified by the results or if they are actually important when modelling subduction. Furthermore, I focused on what happens to the passive margin material throughout the evolution of subduction to investigate under which conditions accretion of the passive margin to the overriding plate is more likely. During subduction, in fact, the margin might decouple, at least in part, from the subducting slab and remain at the surface, or it can completely subduct into the mantle, or partly rising back towards the surface after being subducted (a process known as exhumation). These different dynamics are particularly noticeable when considering the models relative to magma poor and magma rich margins, giving a possible explanation as to why magma poor margins are better preserved than magma rich ones.

1.1 Continental collision and passive margins

The term *continental collision* refers to the closure of an ocean and subsequent mountain building (*Turcotte and Schubert*, 2014 [1]). This process results in the subduction of buoyant continental material, whose positive buoyancy slows down the sinking of the slab in the upper mantle and eventually stops the subduction process (*McKenzie*, 1969 [2], *Cloos*, 1993 [3]). An example of continental collision is showed in figure 1.1 [4].

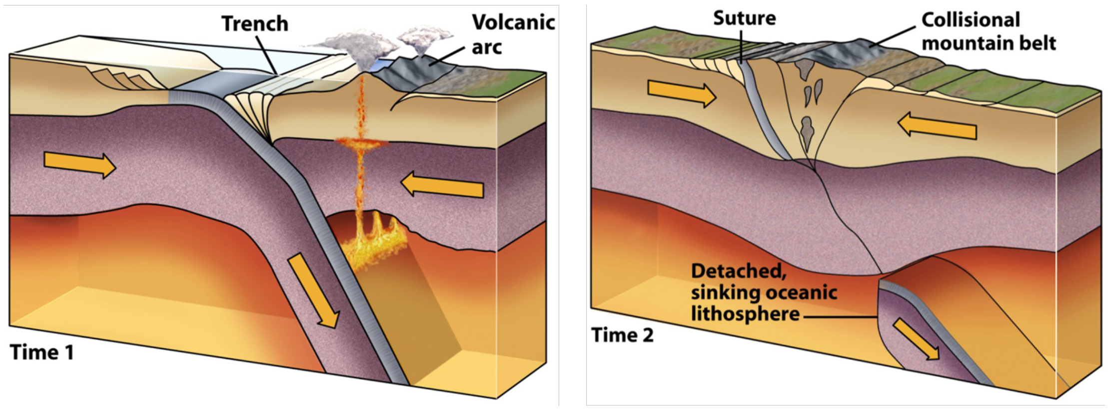

Figure 1.1: Continental collision process, figure from [4]. Subduction is followed by the collision of the continents and, eventually, slab break off. This brings to the formation of a mountain belt.

When the continent arrives at the trench, the continental crust can either subduct, the slab can break-off as a consequence of tensile stress due to the pull of the oceanic lithosphere (which is sinking into the mantle) connected to the continent, or part of the crust can delaminate and accrete on the overriding plate (*Magni et al.*, 2012 [5]).

Various numerical studies have been conducted to investigate different aspects of continental collision. For instance, *Magni et al.*, 2012 [5] looked at the trench migration during continental collision, *van Hunen et al.*, 2011 [7] looked at slab break-off and found that slab strength and crustal density are important for the dynamics of slab break-off, *Baumann et al.*, 2010 [8] investigated the impact of slab age, convergence rate and phase transitions on the viscous mode of slab detachment, and *Toussaint et al.*, 2014 [9] focuses primarily on the influence on subduction of geotherm or thermotectonic age, lower-crustal composition, convergence rate and metamorphic changes in the downgoing crust. However, in general, the details related to passive margins are not taken into account. Indeed, most of these models considered the continental crust to be a structure described by fixed parameters and rheology, which transitions abruptly to oceanic crust. This, however, is not what happens in nature, in which an area of *continent-ocean transition* (COT) is present (*Williams et al.*, 2019 [10]). I therefore decided to try to describe the COT zone, which I refer to as *passive margin*, and I introduced it in my subduction models, in order to understand its significance in the continental collision process. This area is called *passive* because it does not correspond to an active plate margin.

Passive margins are formed during rifting. A representation of this process can be found in figure 1.2, while figure 1.3 gives an overview of the formation of MP and MR margins. Depending on the volumes of extension-related magmatism, two different kinds of margins can be defined: magma poor (MP) and magma rich

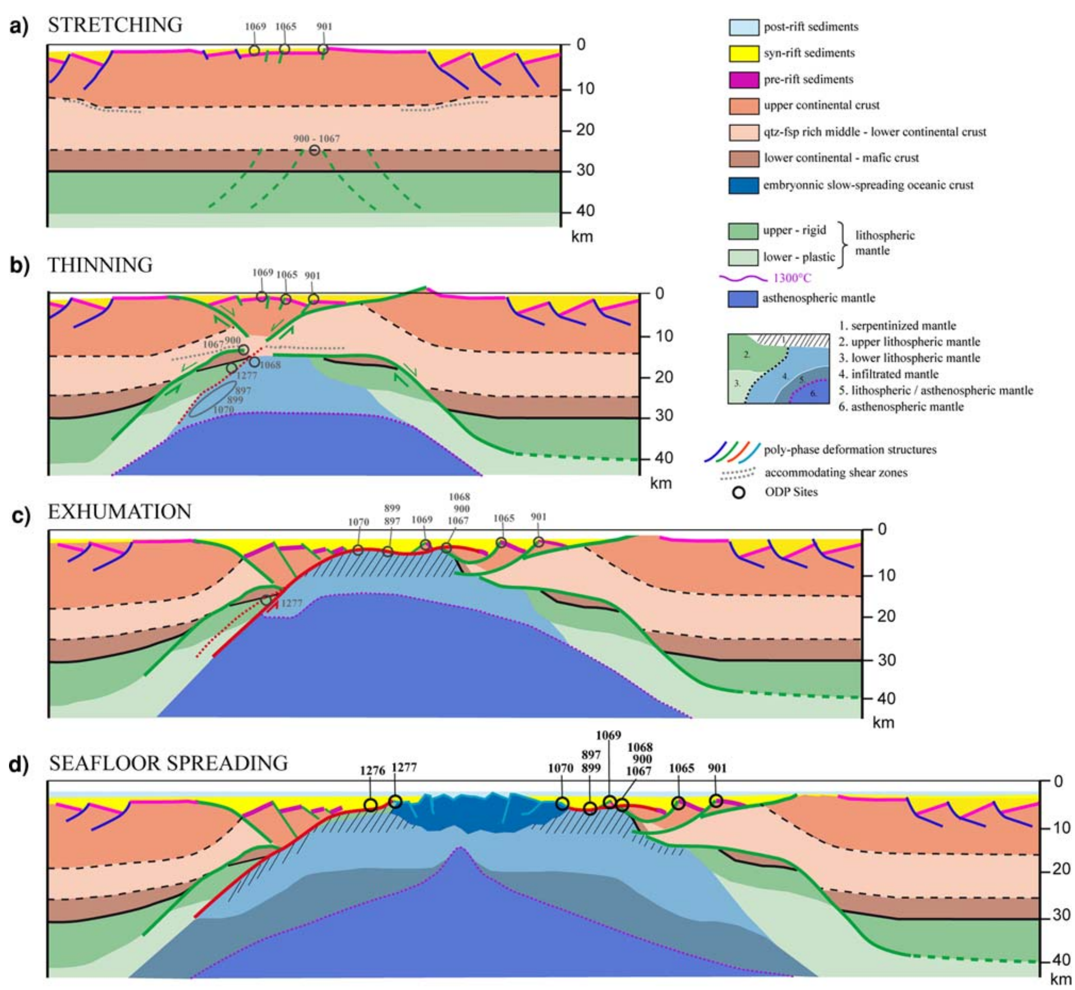

Figure 1.2: Figure from *Péron-Pinvidic and Manatschal*, 2009 [6]: schematic representation of the rifting process, based on observations from the Iberia/Newfoundland rift system. (a) The stretching of the upper crust causes distributed basins; (b)Thinning of the crust to < 10km because of the coupling of deformation in the lower crust and upper and deformation in the upper crust; (c) In some cases exhumation of sub continental mantle may happen; (d) Break up and onset of more or less steady-state seafloor spreading.

(MR) (*Franke*,2013 [11]).

In particular, MP margins are formed when extension is accompanied by magmatism, and they are characterized by stretched and thinned continental crust, while MR margins form when rifting is accompanied by significant mantle melting, with volcanism occurring before and/or during continental breakup (*Franke*, 2013 [11]).

Magma rich margins are characterized by a narrow COT ($50 - 100$ km), and are associated with a thicker-than-normal oceanic crust ($12 - 30$ km, [14]). They contain huge volumes of mafic extrusive and intrusive rocks emplaced in a short period of time (*Callot et al.*, 2002 [15]). MR margins are also composed of a lower crustal body, identified as a high velocity zone (HVZ) for the seismic waves

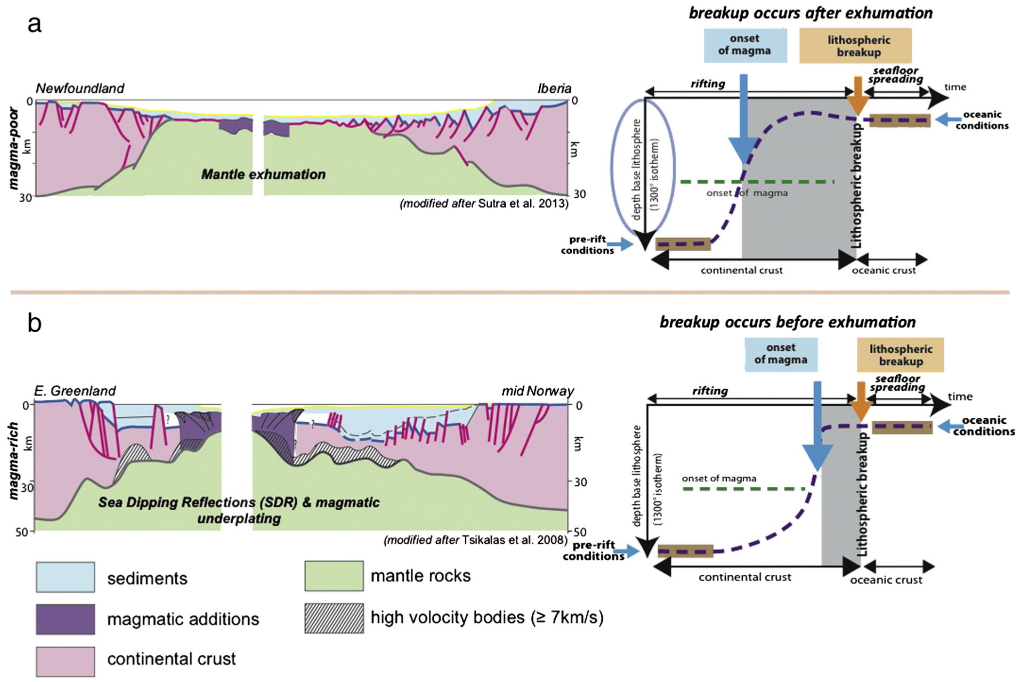

Figure 1.3: Figure from *Manatschal et al.*, 2015 [12]: schematic representation of (a) magma poor and (b) magma rich margins. The diagrams show the evolution of the margins. The vertical axis corresponds to the depth of the lithosphere (defined as the 1300 C isotherm) and the horizontal axis to the time axes, and it shows the evolution of a system from rifting to seafloor spreading. The violet line shows the depth of the lithosphere as a function of time. The green line corresponds to the onset of magma-production that occurs when the lithosphere is thinned to half of its initial thickness. The gray domain corresponds to the time between first production of magma and the lithospheric breakup.At magma poor rifted margins breakup occurs after the mantle has been exhumed, while at magma rich rifted margins, breakup may occur before separation of the two continents.

(v_p > 7.3 km/s [11]) and usually interpreted as bodies of underplated mafic to ultra-mafic magma [14].

Magma poor margins are characterised by a long COT zone (up to 500 km, if not more; *Whitmarsh and Manatschal*, 2001 [16]), composed of highly stretched and thinned continental lithosphere.

Once the collision occurs, there are a few different outcomes for the system, for example formation of an orogen, accretion of part of the continental subducting plate to the overriding plate, or exhumation of continental material after being subducted. All of these processes preserve parts of the subducting plate.

Collision of passive margin is one of the processes responsible for the formation of collisional mountain belts (*Mohn et al.*, 2014 [13]), and are composed by rocks accreted from the lower and/or upper plates. They are heavily influenced by subduction geometry as well as the nature and geological history of converging plates (*Garzanti et al.*, 2007 [17]). This process is showed in figure 1.4.

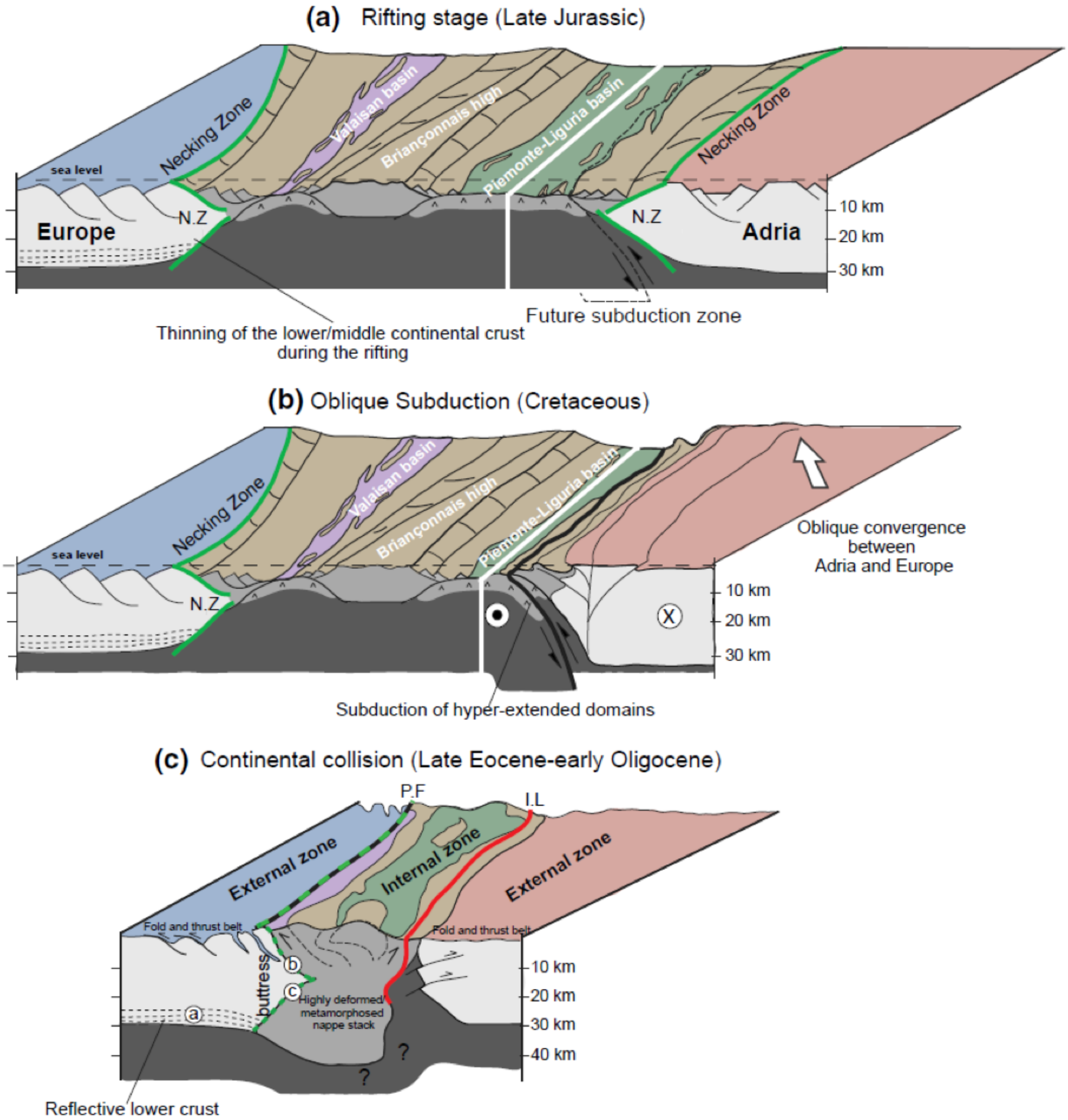

Figure 1.4: Figure from *Mohn et al.*, 2014 [13]: stages of the formation of a mountain belt. The rifting stage (a) is followed by subduction (b), which eventually results in collision (c) and the formation of an orogen.

This process is also linked to the fact that part of the margin material accretes on the overriding plate. Geological observations, in fact, show that passive margin material can be found in mountain belts such as the Alps (*Manatschal and Gianreto*, 2004 [18]).

Furthermore, MP passive margins are more common to observe in mountain belts than MR margins.

Figure 1.5 shows a world map of passive margins today. In this study, in particular, I implemented some models in which I tried to recreate the architecture of the margins described in *Peron-Pinvidic et al., 2013 [19]*, which correspond to the Iberia-Newfoundland conjugate margin (magma poor; *Peron-Pinvidic et al.*, 2009 [6]), the mid-Norwegian-central East Greenland conjugate margin (magma rich; *Geoffroy*, 2005 [14]) and the Angola-Esperito Santo conjugate margin (magma poor; *Peron-Pinvidic et al., 2013 [19]*), identified in figure 1.6. Moreover, I implemented passive margins in the models with a more simplified structure, which allowed me to perform a parametric study and systematically investigate the effects of each feature on the dynamics of collision.

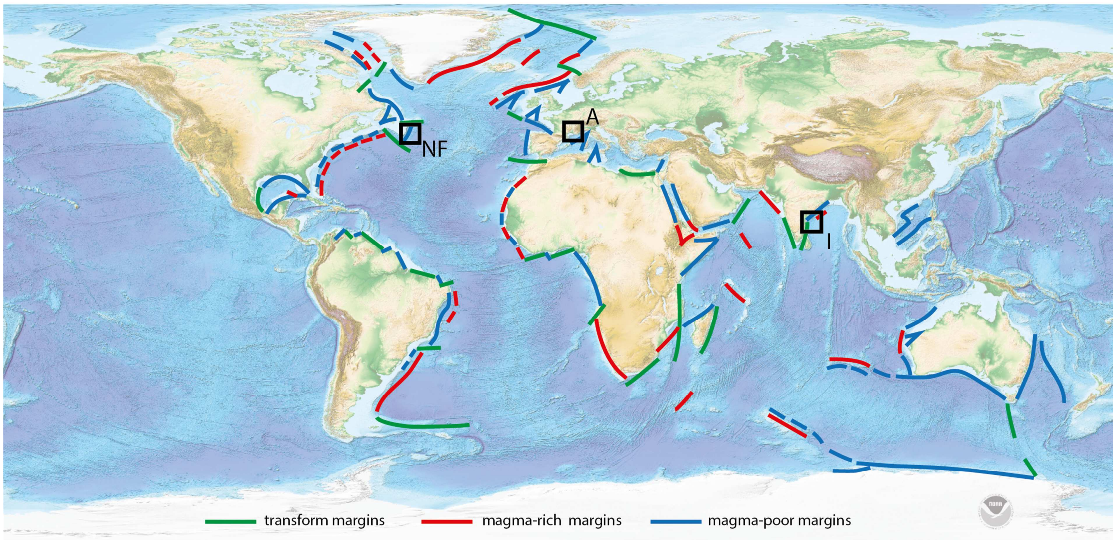

Figure 1.5: Figure from *Haupert et al.*, 2016 [20]. World map of modern passive margins. The red line identifies magma rich passive margins, while the blue line identifies magma poor ones.

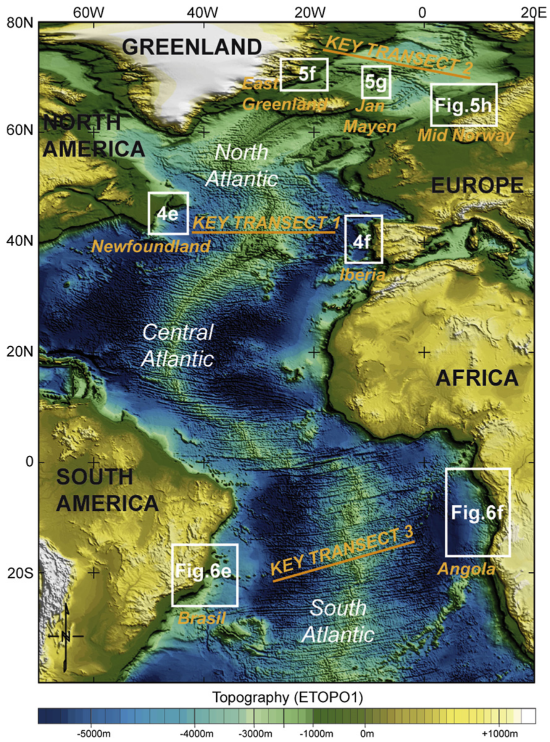

Figure 1.6: Figure from *Peron-Pinvidic et al.*, 2013 [19]. Topographic map of the Atlantic Ocean. The boxes show the location of the passive margins we described in this study.

Chapter 2

Methodology

2.1 The subduction problem

Subduction processes can be described in terms of thermal and compositional convection. Mantle convection, in fact, is strongly linked to plate motion and is driven by the internal buoyancy, which derives by density variations. These density variations are mainly due to the composition and thermal state of the system, and they can be described as follows:

$$\Delta\rho(T, C) = \rho_0 \left[\frac{\Delta\rho_c}{\rho_0} - \alpha(T - T_0) \right] \qquad , \tag{2.1}$$

with symbols and their values described in table 2.3.

From a thermal point of view, the density difference is described through the thermal expansion α, which means that if temperature decreases, density increases. When modelling subduction, therefore, we can describe a tectonic plate as a layer with temperature varying from a surface value to a mantle reference value. This means that a subducting plate can be considered as a cold and dense layer, which has a negative buoyancy and, thus, sinks into the mantle.

The compositional density variation, on the other hand, is due to the presence of different materials. In this study, I distinguish between continental crust ($\rho_c =$ 2700 kg/m^3, 2800 kg/m^3 and 2900 kg/m^3), oceanic crust ($\rho_o =$ 3000 kg/m^3), and mantle ($\rho_{mantle} =$ 3300 kg/m^3).

2.1.1 Governing equations

When describing the thermal and compositional convection in the mantle, the equations that have to be taken into account are those for the conservation of mass, momentum, energy and composition.

I consider the mantle to be an incompressible and viscous medium, for which the Boussinesq approximation holds (i.e., the density variations are neglected except in the buoyancy term of the conservation of momentum equation except for the gravity term, which is linked to the buoyancy). All the equations presented in this section, therefore, are subject to this approximation.

For an incompressible fluid, the conservation of mass (whose general equation is $\partial\rho/\partial t + \boldsymbol{\nabla}\cdot(\rho\boldsymbol{u}) = 0$) is reduced to the description of a divergence-free velocity field:

$$\boldsymbol{\nabla}\cdot\boldsymbol{u} = 0 \tag{2.2}$$

The conservation of momentum, which represent the balance between pressure, viscous and body forces in the system, can be described thanks to the Stokes equations:

$$\boldsymbol{\nabla}p - \boldsymbol{\nabla}\cdot\boldsymbol{\tau} = \Delta\rho\boldsymbol{g} \tag{2.3}$$

The conservation of energy is described as an equation for the temperature field:

$$\frac{\partial T}{\partial t} + \boldsymbol{u}\cdot\boldsymbol{\nabla}T = k\boldsymbol{\nabla}^2 T \tag{2.4}$$

The conservation of composition is described by a purely advective transport equation:

$$\frac{\partial C}{\partial t} + \boldsymbol{u}\cdot\boldsymbol{\nabla}C = 0 \tag{2.5}$$

This set of equations can be rendered non-dimensional thanks to the following scaling expressions:

$$\boldsymbol{x} = \boldsymbol{x}'h \qquad t = t'h^2/k \qquad \boldsymbol{u} = \boldsymbol{u}'k/h \qquad T = \Delta T(T' + T_0) \qquad \eta = \eta_0\eta' \tag{2.6}$$

This set of non-dimensional equations can therefore be rewritten as (dropping the primes for legibility):

$$\boldsymbol{\nabla}\cdot\boldsymbol{u} = 0 \qquad , \tag{2.7}$$

$$-\boldsymbol{\nabla}p + \boldsymbol{\nabla}\cdot[\eta(\boldsymbol{\nabla}\boldsymbol{u} + \boldsymbol{\nabla}^T\boldsymbol{u})] + (RaT + RbC)\boldsymbol{e}_z \qquad , \tag{2.8}$$

$$\frac{\partial T}{\partial t} + \boldsymbol{u}\cdot\boldsymbol{\nabla}T = \boldsymbol{\nabla}^2 T \qquad , \tag{2.9}$$

$$\frac{\partial C}{\partial t} + \boldsymbol{u}\cdot\boldsymbol{\nabla}C = 0 \qquad , \tag{2.10}$$

where I have introduced the thermal Rayleigh number:

$$Ra = \frac{\alpha\rho_0 g\Delta T h^3}{k\eta_0} \qquad , \tag{2.11}$$

and the compositional Rayleigh number:

$$Rb = \frac{\delta \rho_c g h^3}{k \eta_0} \qquad , \tag{2.12}$$

which control the vigour of convection.

The symbols in the previous equations are described in table 2.3

2.2 Numerical modelling: Citcom

The governing equations above are solved with the Finite Element Method (FEM), using the parallel finite element code Citcom (*Moresi and Solomatov*, 1995 [21], *Zhong et al.*, 2000 [22]).

I used the Eulerian finite element technique for the conservation of mass, momentum and energy, and the Lagrangian tracer particle method for the transport of composition. The difference between the two is the reference system. For the Eulerian method, I calculated the flow field and the fluid properties relative to a fixed point in space, whereas for the Lagrangian method we use a coordinate system in which the velocities of the particles of the flow are relative to the position of the single particles.

The governing equations are partial differential equation (PDE). The FEM is one of the most common ways to solve this kind of equations, in that it allows to transforms the PDE in an approximate system of ordinary differential equations (ODEs) that can subsequently be solved using standard techniques. In order to do that, I discretized the model domain into a finite number of elements (a mesh) inside which the ODEs can be solved thanks to a fourth order Runge-Kutta integration.

I considered a mesh with variable elements dimensions. The simpler models I implemented have bigger mesh elements. When I introduced the oceanic crust and high viscosity contrasts, however, I had to refine the mesh and consider smaller elements in some areas of our domain. The mesh resolutions are reported in table 2.1 and 2.2.

Moreover, the FEM can be used to solve problems which involve complex geometries, inhomogeneities in the domain or strong variations of the properties of the material. Therefore, it is especially suitable to describe subduction processes, in which all of the situations above are present.

Using the procedure described in *Moresi and Solomatov* [21], the equations for the conservation of mass (2.7) and momentum (2.8) can be discretized and rewritten as:

$$Au + Bp = f \qquad , \tag{2.13}$$

Reference model mesh				
Coordinate	**Number of layers**	**Upper bound of the mesh region**	**Number of nodes per region**	**Mesh resolution** (km)
x	5	0.06 2.21 3.37 4.94 5.0	6 132 155 102 6	7.92 10.83 4.97 10.26 7.92
z	2	0.33 1.0	27 36	8.38 12.63

Table 2.1: Mesh employed when studying the reference model.

Refined mesh				
Coordinate	**Number of layers**	**Upper bound of the mesh region**	**Number of nodes per region**	**Mesh resolution** (km)
x	5	0.06 2.21 3.37 4.94 5.0	6 132 155 102 6	7.92 10.83 4.97 10.26 7.92
z	2	0.68 1.0	155 37	2.91 5.87

Table 2.2: Mesh employed when I introduced the oceanic crust and high viscosity contrasts. I refined the first 450 km along the z-axis, in order to be able to resolve small structures even during the break-off.

$$B^T u = 0 \qquad , \tag{2.14}$$

where u is a vector of unknown velocities, A is the "stiffness" matrix, B is the discrete gradient operator, p is a vector of unknown pressures, and f is a vector which represents the body forces acting on the fluid. The coefficients of A, B and f are obtained using a standard finite element formulation with linear velocity and constant shape functions. By multiplying 2.13 for $B^T A^{-1}$ and using 2.14, the following equation can be obtained, in which the unknown velocity vector does not appear:

$$B^T A^{-1} B p = B^T A^{-1} f \tag{2.15}$$

This equation is a form of the Uzawa algorithm and can be solved with an iterative conjugate gradient method, while the equation 2.9 for the conservation of energy is solved with a standard Petrov-Galerkin method (*Yu et al.*, 1987 [23]).

Compositional properties In order to model the presence of different compositions and transport their properties through the computational domain in a time dependent model as described in equation 2.10, the Lagrangian tracer particle method has been used (*Di Giuseppe et al.*, 2008 [24], *van Huen et al.*, 2002 [25]). Initially, a large number of tracers (more than 40 per element) is distributed randomly in the model domain. The composition function C can hold on of two values:

$$C = \begin{cases} 1 & \text{for the continental (or oceanic) crust} \\ 0 & \text{for the mantle material} \end{cases} \tag{2.16}$$

At each time step, the tracers are advected with the flow field, and the interpolation of the compositional information is done for every element, and is applied to the integration points in order to obtain a new distribution of tracers. This distribution is then used to determine the density of the material and the buoyancy forces.

2.3 Rheology

An important aspect of subduction models is the rheology of the various components of the process that must be taken into account. Indeed, differences in rheological properties reflect on the processes that we consider in this work, such as continental subduction, exhumation, and slab break-off.

In this section, therefore, I describe the rheologies that I used to model mantle, lithosphere and passive margins.

2.3.1 Mantle rheology

On geological time scales, the mantle behaves like a fluid. On the first order, it can be considered as a Newtonian fluid. However, in order to model a more realistic behaviour, I used a temperature and stress dependent viscosity. Furthermore, laboratory studies show that the main sources of deformation for the mantle minerals are the diffusion creep and the dislocation creep (*Ranalli*, 2000 [26]).

In general, the strain rate for a solid-state creep process in the mantle is (*Karato and Wu*, 1993 [27]):

$$\dot{\epsilon} = A\tau^n d^{-m} e^{-\frac{E+pV}{RT}} \quad , \tag{2.17}$$

whose symbols are described in table 2.3.

Knowing that viscosity and strain rate are linked by $\eta = \tau/\dot{\epsilon}$, we can rewrite equation 2.17 as:

$$\eta = A^{-1/n}\dot{\epsilon}^{(1-n)/n}d^{m/n}e^{-\frac{E+pV}{RT}} \tag{2.18}$$

Depending on the creep mechanism, the parameters $mandn$ hold different values. In particular:

- Diffusion creep (diffusion of vacancies through grains): the stress dependence is linear ($n = 1$);
- Dislocation creep (motion of dislocations through grains): nonlinear stress dependence ($n = 3 - 5$) and no grain size dependence ($m = 0$).

The values I used in this work can be found in table 2.3.

Because of the Boussinsq approximaton, the activation volume V is zero.

We can rewrite the equation 2.18 as:

$$\eta = A_D\dot{\epsilon}^{(1-n)/n}e^{-\frac{E}{RT}} \tag{2.19}$$

where $A_D = A^{-1/n}d^{m/n}$.

Since both creep mechanisms discussed above take place in the mantle, I considered an effective viscosity η_{eff} that, at each point, is defined as:

$$\eta_{eff} = min\{\eta_{diff}, \eta_{disl}\} \tag{2.20}$$

where η_{diff} is the viscosity described by the diffusion creep law and η_{disl} the one derived for the dislocation creep.

A reference value for the viscosity of the upper mantle does not exist due to the uncertainties in the indirect measurements. The best estimates are derived from postglacial rebound models, which suggest a value $\eta_{mantle} = (3.6 \pm 1) \cdot 10^{20}$ Pa s (*Lambeck and Johnston*, 1998 [28]). In my models, I use the approximated reference value 10^20 Pa s, which, however is not a fixed value, but it changes following the law described in equation 2.20.

2.3.2 Lithosphere rheology

The lithosphere can deform both in a brittle and ductile fashion, depending on its composition, depth, temperature, and stresses. In fact, overall we can consider it to be ductile at depth, since the pressure and temperature increase with it, while it generally behaves as brittle near the surface. This kind of behaviour is summarized in figure 2.1.

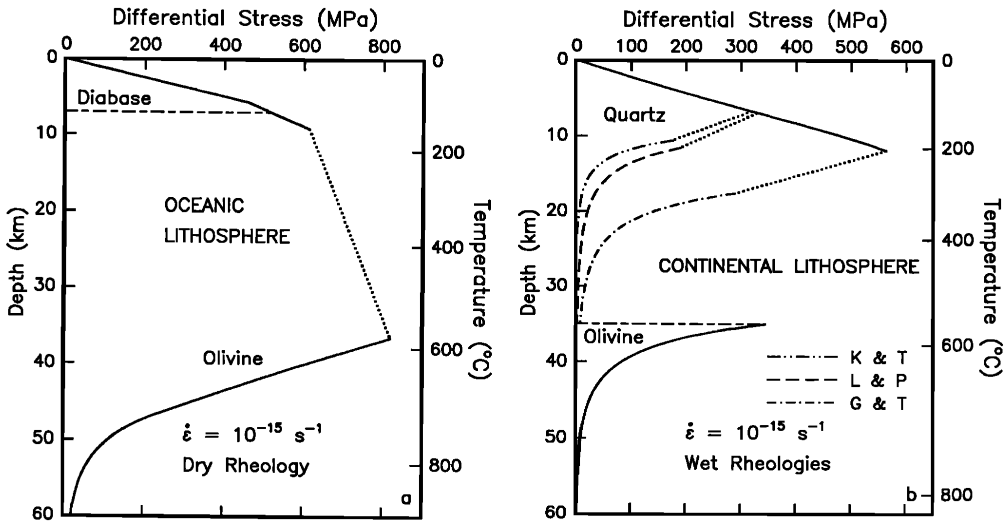

Figure 2.1: Figure from *Kohlstedt et al.*, 1995 [29]. The strength envelopes for the oceanic and continental lithosphere show the shallow brittle behaviour and deep ductile behaviour of the crust.

The ductile behaviour can be modeled with the same laws used for the mantle. Near the surface, however, the lithosphere behaviour is brittle, and it has to be treated differently. The law that describes this behaviour is

$$\eta = \frac{\tau_y}{2\dot{\epsilon}} \qquad , \tag{2.21}$$

where τ_y is the yield stress and it is described as:

$$\tau_y = min\{\tau_0 + \mu p_0, \tau_{max}\} \tag{2.22}$$

τ_{max} represents the maximum yield stress and $\tau_0 + \mu p_0$ is the Bayerlee law (*Byerlee*, 1978 [30]), where τ_0 is the stress at the surface, μ the friction coefficient and p_0 the lithostatic pressure. The effective viscosity is computed with equation 2.21. Since the viscosity depends strongly on the temperature, in order not to have non-physical strength at the surface, where the temperature is $T = 0$ °C, I imposed a maximum viscosity value η_{max}. At each point of the finite element grid, the effective viscosity is the minimum value of all those computed above.

2.3.3 The subduction thrust fault and the mantle wedge

Between the plates, large stresses are localized and a strong deformation occurs. Near the surface, this results in the strain being accommodated by earthquakes in major faults or shear localization. In order to model this feature and to have decoupling between the plates, a narrow weak zone (20 km wide, 50 km deep, with viscosity 10^{20} Pa s and fixed radius of 0.8) is imposed.

At depths of $50 - 150$ km, the slab dehydrates due to high temperature and pressure that cause the subducting oceanic slab, which has a higher water content than the continental one, to release water through metamorphic reactions (e.g., Schimdt and Poli, 1998). The fluids released from the slab trigger partial melting and, thus, weaken the mantle wedge above it (e.g., Ringwood, 1974). This process is simulated by the presence of a mantle wedge, which is a weak zone about 200 km wide and reaches a depth of 150 km below the overriding plate. The viscosity of the mantle wedge is 10^{20} Pa s.

These two features move consistently with the slab, following the dynamics of the system.

2.3.4 Passive margin rheology

Since the aim of this work is to understand how different types of passive margins can affect the subduction dynamics, special attention has been paid to the way they are implemented in the models. When it comes to the rheology (as seen in Chapter 1), the magma poor (MP) and magma rich (MR) passive margins are different.

Magma poor margins are characterized by a long (up to 500 km, if not more) transitional zone between the continent and the ocean composed of highly stretched and faulted continental lithosphere. Therefore, I considered this region to be weaker than he surrounding material.

On the other hand, magma rich margins have a shorter transition zone composed of newly formed volcanic rocks: a thick layer of oceanic crust at the surface and, below it, a 'lower crustal body' that is likely to be the dense and strong residue material.

A schematic representation of these two types of margins can be found in figure 2.2.

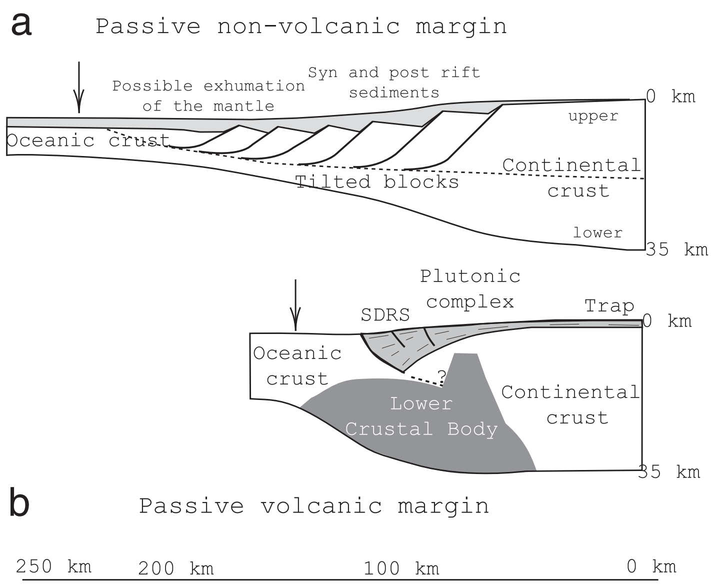

Figure 2.2: Figure from *Callot et al.*, 2002 [15]. Schematic representation of (a) magma poor and (b) magma rich passive margins. The arrow indicates the continent-ocean boundary.

2.4 Model setup

The staring point for this work is based on the model described in *Magni et al.* [5], and is depicted in figure 2.3.

The reference model describes a geometry with an abrupt transition between continent and ocean. This means that in the reference case we are not considering the presence of a passive margin.

I studied this case as a starting point, in order to understand, first of all, what happens if the passive margin is not taken into account, and, secondly, what the differences in the subduction process are when I add one.

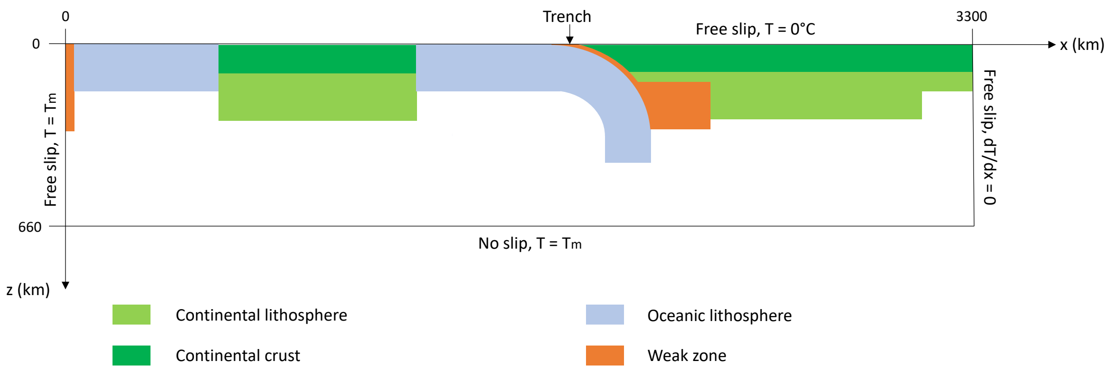

Figure 2.3: Schematic representation (not to scale) of the initial setup of the reference model, with the boundary conditions and the dimensions.

Subduction is modeled in a 2D rectangular domain, in the plane xz. The upper limit of the domain, along the z-axis, represents the Earth's surface (I am not taking into account the presence of the ocean), while the bottom of the domain represents the upper-lower mantle boundary at 660 km.

For all the models presented in this work, the aspect ratio is 1 : 5.

The initial setup, described in figure 2.3, can be summarized as follows:

- The overriding plate is entirely composed by continental lithosphere, with continental crust present along the whole plate.

- The subducting plate is described as a oceanic lithosphere which presents a continental block (composed by a continental crust and lithosphere) of about 800 km. This block is located at a distance of about 500 km from the position of the trench. At the trench, the lithosphere reaches a depth of 300 km with a curvature radius of 500 km as this provides enough slab pull to initiate subduction, without the need to impose external forces to push the plates.

- A weak zone, corresponding to an area with low viscosity (10^{20} Pa s), has been introduced at the left top corner, in order to facilitate the motion of the subducting plate as a consequence of the velocity flux in the mantle.

- A narrow low viscosity zone (10^{20} Pa s), which reaches a depth of about 50 km has been introduced along the subducting plate at the trench, in order to be able to decouple the two plates throughout the entire subduction process. The shape of this low viscosity zone remains fixed during the whole process, but its position changes according to the position of the slab.

- A 100 km high and 200 km wide mantle wedge, with the same viscosity as the other weak zones, has been introduced at a depth of 50km at the trench, to simulate the weakening of the area above the slab because of the mantle hydration and melting (*Billen and Gurnis, 2001* [31]; *van Hunen and Allen, 2011* [7]). The shape of the mantle wedge is a function of the slope of the slab and is, therefore, not fixed.

- The initial thermal structure of the oceanic lithosphere is assumed to be the half-space cooling model for a 50 Myr plate (*Turcotte and Schubert, 2014* [1]). For the continental lithosphere, the temperature increases linearly from 0 °C at the surface to the mantle temperature T_m = 1350 °C at a depth of 150 km.

- The boundary conditions for the temperature require to have 0 °C at the surface, dT/dx=0 at the right boundary, and T_m = 1350 °C at the lower and left boundary.

- I impose the boundary conditions for the velocity to be free-slip everywhere but at the lower boundary, where we have a no-slip boundary condition. The assumption taken here is that because of its high viscosity, the lower mantle acts as a rigid boundary.

In the reference model, the only type of crust taken into account is the continental one. In other models, depending on the characteristics of the margin, I add an oceanic crust. In all the models I implemented, the bottom of the lithospheric mantle of the passive margin follows the same geometry of the crustal part.

2.5 Modelling Passive Margins

In order to describe the two types of passive margins described in section 2.3.4, I started from the reference model described in section 2.4 and we progressively added features until we managed to describe, respectively, magma poor and magma rich margins.

In this section I describe the main types of margins that have been the intermediate and then final steps in our study of passive margins. In my parametric study, I focus on the geometry, density, and rheology of the passive margin as they are likely to play key roles in the dynamics of continental collision.

The results and comparison between the models are presented, respectively, in Chapter 3 and 4.

2.5.1 Reference models: abrupt transition between continental and oceanic lithosphere

I first performed a parametric study with a set of models similar to the one described in section 2.4, changing some key properties of the continental crust, such as its density and its thickness.

The continental crust geometry is described in figure 2.4.

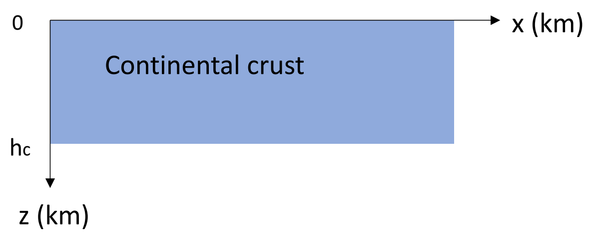

Figure 2.4: Schematic representation of the models in which we did not take the passive margin into account. h_c represents the crustal thickness.

In these models there is an abrupt transition between continental and oceanic crust, and this results in the absence of a passive margin.

The values of the parameters for the continental crust in these models are:

- Crustal thickness: $h_c = 30\ \mathrm{km}, 35\ \mathrm{km}, 40\ \mathrm{km}$;
- Crustal density: $\Delta\rho_c = 400\ \mathrm{kg/m^3}, 500\ \mathrm{kg/m^3}, 600\ \mathrm{kg/m^3}$;
- Maximum viscosity: $\eta_c = 20^{23}\ \mathrm{Pa\,s}$.

2.5.2 Passive margins with a ramp-type geometry of variable length and height

The first step I took to introduce a more realistic passive margin is to add one with a ramp type geometry, as described in figure 2.5.

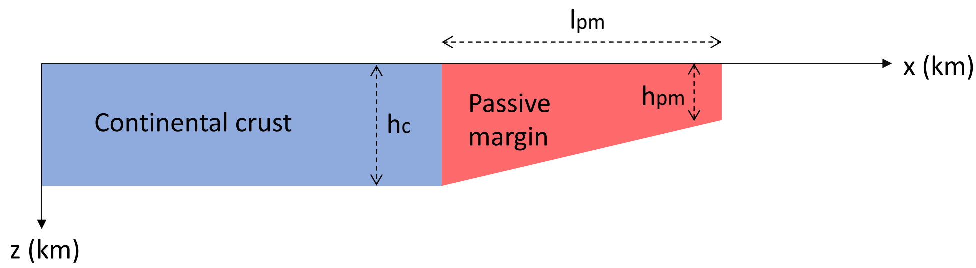

Figure 2.5: Schematic representation of the models in which the margin has a ramp-type geometry. h_c represents the crustal thickness, h_{pm} the final thickness of the margin and l_{pm} the length of the margin.

The geometry of the margin is defined by the following function:

$$z_{margin} \leq h_c - \left(\frac{h_c}{2}\right) \cdot \left(\frac{x - x_{min}}{x_{max} - x_{min}}\right) \tag{2.23}$$

where x_min and x_max are, respectively, the starting and ending points of the margin on the x- axis, and z_{margin} is the margin thickness along the whole interval, with:

$$z_{margin}(x_{min}) = h_c \qquad z_{margin}(x_{max}) = h_m \tag{2.24}$$

In these models, I decided to consider the following values for the crustal parameters:

- Crustal thickness: $h_c = 40\ \mathrm{km}$;
- Crustal density: $\Delta\rho_c = 500\ \mathrm{kg/m^3}$;
- Final thickness of the margin: $h_m = 0\ \mathrm{km}, 20\ \mathrm{km}$;

- Margin length: $l_m = 50$ km, 100 km, 150 km, 200 km;
- Maximum viscosity of the margin: $\eta_c = \eta_m = 20^{23}$ Pa s.

2.5.3 Adding an oceanic crust

Since magma rich passive margins are characterized by a thicker-than-normal oceanic crust, we decided to add an oceanic crust to our geometry models, as represented in figure 2.6.

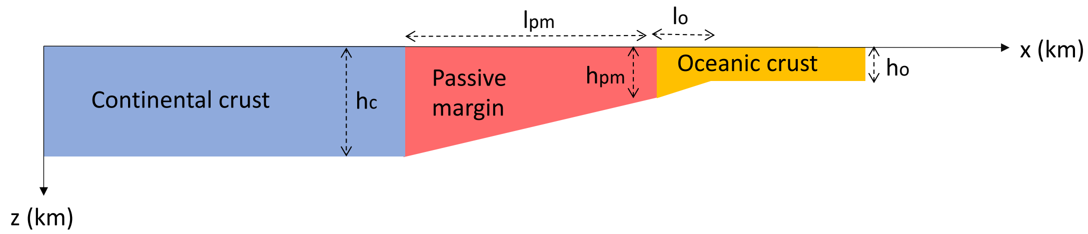

Figure 2.6: Schematic representation of the models in which the margin has a ramp-type geometry and an oceanic crust is considered. h_c represents the crustal thickness, h_m the final thickness of the margin, l_m the length of the margin, h_o the final thickness of the ocean and l_o the length of the oceanic ramp.

The parameters which describe the crust in these models have the following values:

- Crustal thickness: $h_c = 30$ km;
- Crustal density: $\Delta\rho_c = 500$ kg/m^3;
- Oceanic crust density:$\Delta\rho_o = 300$ kg/m^3;
- Final thickness of the margin: $h_m = 20$ km;
- Final oceanic thickness: $h_m = 0$ km, 7 km;
- Margin length: $l_m = 50$ km;
- Average oceanic crustal thickness: $\bar{l_o} = 0$ km, 7 km, 13.5 km, 20 km
- Maximum viscosity of the margin: $\eta_c = \eta_m = 20^{23}$ Pa s.

The oceanic crust has been considered as present in the first 40 km of our domain, since at this depth the transition from basalt to eclogite occurs. From this point on, the density of the oceanic crust is the same as the density of the mantle.

2.5.4 Magma Poor margins

As described in section 2.3.4, a magma poor passive margin is characterized by a weaker rheology. In order to model this feature, I ran a set of models with different (lower) viscosity values of the whole margin. Figure 2.7 shows the characteristics we implemented for magma poor margins.

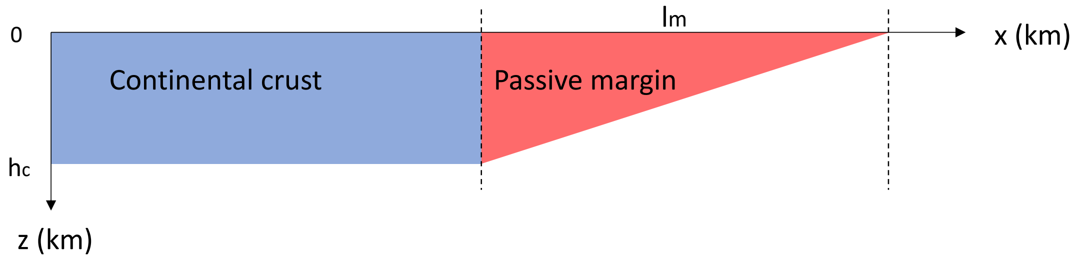

Figure 2.7: Schematic representation of a magma poor margin. h_c represents the crustal thickness and l_m the length of the margin. The oceanic crust is not taken into account here.

In this case, the parameters which describe the margin are:

- Crustal thickness: $h_c = 30$ km;
- Crustal density: $\Delta\rho_c = 500$ kg/m^3;
- Final thickness of the margin: 0 km;
- Margin length: $l_m = 100$ km, 200 km, 300 km, 100 km, 400 km, 500 km;
- Maximum viscosity of the margin: $\eta_m = 5{\cdot}10^{20}$ Pa s, 10^{21} Pa s, $5{\cdot}10^{21}$ Pa s, 10^{22} Pa s, $5{\cdot}10^{22}$ Pa s, 10^{23} Pa s.

2.5.5 Magma Rich margins

Magma rich margins have more complicated complicated structure than the magma poor ones and, thus, I implemented them in various steps. Here we present only the final step (figure 2.8), which better represents the MR margin described in figure 2.2. A complete description of all the other steps is presented in figure 4.9.

Here I describe the margin as the sum of more elements. The continental crust is described by a step function, and part of it composes the MR margin, as well as the oceanic ramp and the lower crustal body.

The lower crustal body corresponds to a high velocity zone (HVZ) for the seismic waves, which is interpreted to be dense and possibly stronger material (in this work, I assumed this lower crustal body to be stronger than the rest of the crust, but the rheology of this area is not known exactly (*Stab et al.*, 2016 [32]);

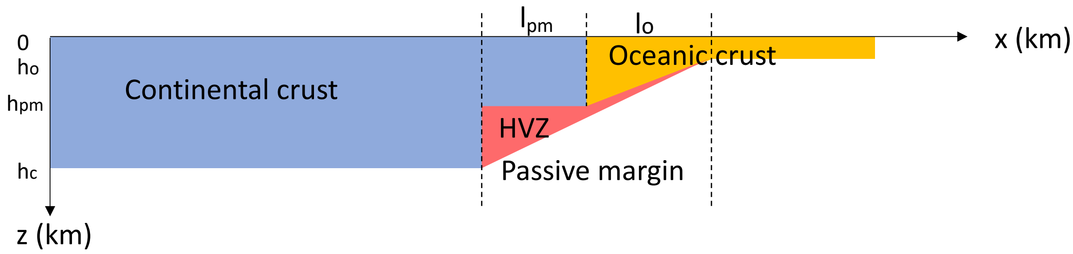

Figure 2.8: Schematic representation of a magma rich margin. h_c represents the crustal thickness, h_m the final thickness of the crust, l_m the length of the crustal step and l_o the length of the oceanic ramp. The red area represents the lower crustal body (labeled as HVZ, i.e. the high velocity zone for the seismic waves) described in figure 2.2.

this point will be further discussed in Chapter 5). Therefore, I implement it in the models as an area with higher viscosity and higher density than the rest of the margin. In addition to the geometry, I vary the viscosity and density values of this body to study their effects on the dynamics of continental collision.

The values of the parameters for a magma rich margin as the one in figure 2.8 are:

- Crustal thickness: $h_c = 40$ km;
- Crustal density: $\Delta\rho_c = 500$ kg/m^3;
- Oceanic crust density: $\Delta\rho_o = 300$ kg/m^3;
- HVZ density: $\Delta\rho_{HVZ} = 0$ kg/m$^3, -100$ kg/m$^3, -200$ kg/m^3;
- Final crustal thickness: $l_m = 20$ km;
- Final oceanic thickness: $h_m = 7$ km;
- Margin length: $l_m = 50$ km, 100 km;
- Average oceanic crustal thickness: $\bar{l_o} = 13.5$ km
- Maximum viscosity of the HVZ: $\eta_{HVZ} = 10^{24}$ Pa s.

Parameter	**Symbol**	**Value**	**Unit**
Rheological pre-exponent	A_D	6.52×10^6	$[\mathrm{Pa}^{-n}\mathrm{s}^{-1}]$
Composition parameter	C	$-$	$[-]$
Grain size	d	$-$	$[m]$
Activation Energy	E	360	[kJ/mol]
Vertical unit vector	$\boldsymbol{e}_z$	$-$	$[-]$
Gravitational acceleration	g	9.8	$[\mathrm{m/s}^2]$
Height of the domain	h	660	[km]
Thermal diffusivity	k	10^{-6}	$[\mathrm{m}^2/\mathrm{s}]$
Grain size exponent	m	$-$	$[-]$
Rheological power law exponent	n	$1(\text{diff.c.}), 3.5(\text{disl.c.})$	$[-]$
Deviatoric pressure	p	$-$	[Pa]
Lithostatic pressure	p_0	$-$	[Pa]
Gas constant	R	8.3	[J/Kmol]
Thermal Rayleigh number	Ra	4.4×10^6	$[-]$
Compositional Rayleigh number	Rb	1.7×10^7	$[-]$
Temperature	T	$-$	[°C]
Time	t	$-$	[s]
Absolute temperature	T_{abs}	$-$	[K]
Reference temperature	T_m	1350	[°C]
Velocity	u	$-$	[m/s]
Activation volume	V	$-$	$[\mathrm{m}^3/\mathrm{mol}]$
Thermal expansion coefficient	α	3.5×10^{-5}	$[\mathrm{K}^{-1}]$
Density variation	$\Delta\rho$	$-$	$[\mathrm{kg/m}^3]$
Compositional density constant	$\Delta\rho_c$	$-$	$[\mathrm{kg/m}^3]$
Strain rate	$\dot{\epsilon}$	$-$	$[\mathrm{s}^{-1}]$
Viscosity	η	$-$	[Pa s]
Reference viscosity	η_0	10^{20}	[Pa s]
Maximum lithosphere viscosity	η_{max}	$10^{22} - 10^{24}$	[Pa s]
Friction coefficient	μ	$0 - 0.1$	$[-]$
Reference density	ρ_0	330	$[\mathrm{kg/m}^3]$
Stress	σ	$-$	[Pa]
Deviatoric stress	τ	$-$	[MPa]
Surface yield stress	τ_0	$40 - 200$	[m Pa]
Maximum yield stress	τ_{max}	$200 - 400$	[m Pa]
Yield stress	τ_y	$-$	[m Pa]

Table 2.3: Parameters, symbols and units used in the equations presented in this Chapter.

Chapter 3

Models description

The aim of this chapter is to present results of the main types of geometries and rheologies that were chosen in order to study the effect of passive margins on the continental collision dynamics and to briefly describe the subduction process for every margin type.

The reference model (whose initial setup is described in Chapter 2) is based on the one described in *Magni et al.*, 2012 [5], and, starting from this one, other geometries were implemented at first, followed by models in which the rheology was changed.

A list of the models studied and their details can be found in appendix A.

3.1 Reference models: abrupt transition between continental and oceanic lithosphere

The time evolution of the reference model (figure 2.3) is presented in figure 3.1.

The subduction process follows some steps. At first the oceanic lithosphere sinks into the upper mantle and the slab reaches the bottom of the computational domain, which represent the upper-lower mantle discontinuity. Afterwards, the slab starts to flatten on the bottom of the domain. Continental collision happens about 10 Myr after the beginning of the model. This causes subduction to slow down due to the fact that the continent is lighter and more buoyant than the ocean and it resists subduction. At depth, however, the oceanic part of the slab is still pulling down. These two opposite forces creates high stresses within the slab that weaken it and necking of the slab occurs. Finally, the slab breaks-off at about 20 Myr detaching the continental part of the subucting plate from the oceanic one, which continues to sink into mantle.

In all the models presented in this work, the subduction dynamics are the same as the ones described here.

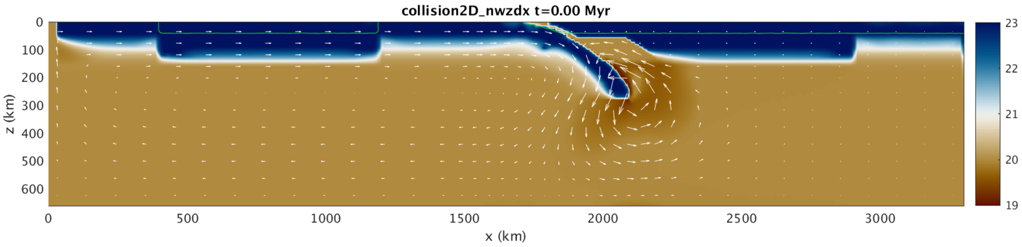
collision2D_nwzdx t=0.00 Myr
z (km)
x (km)
0 100 200 300 400 500 600
0 500 1000 1500 2000 2500 3000
19 20 21 22 23

(a)

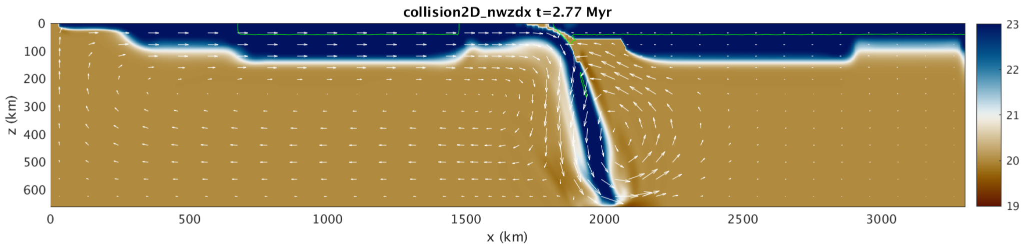
collision2D_nwzdx t=2.77 Myr
z (km)
x (km)
0 100 200 300 400 500 600
0 500 1000 1500 2000 2500 3000
19 20 21 22 23

(b)

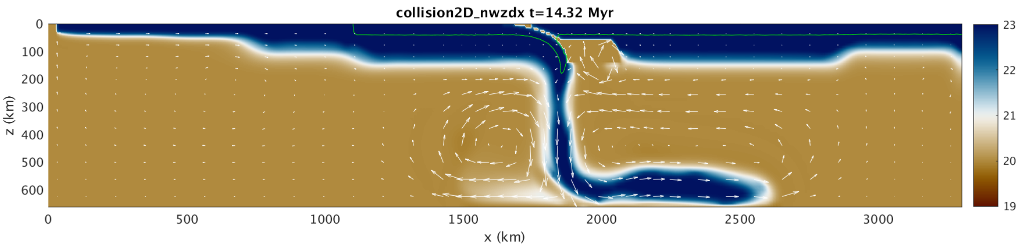
collision2D_nwzdx t=14.32 Myr
z (km)
x (km)
0 100 200 300 400 500 600
0 500 1000 1500 2000 2500 3000
19 20 21 22 23

(c)

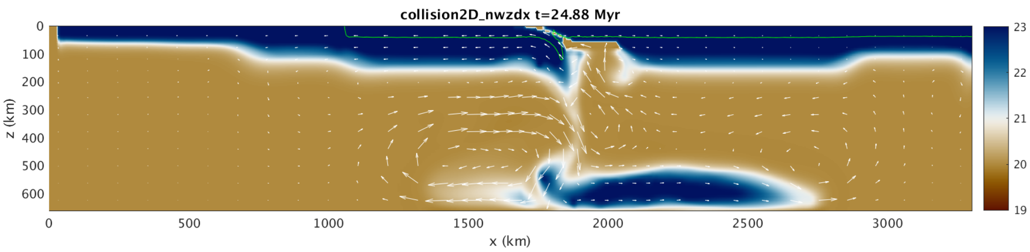
collision2D_nwzdx t=24.88 Myr
z (km)
x (km)
0 100 200 300 400 500 600
0 500 1000 1500 2000 2500 3000
19 20 21 22 23

(d)

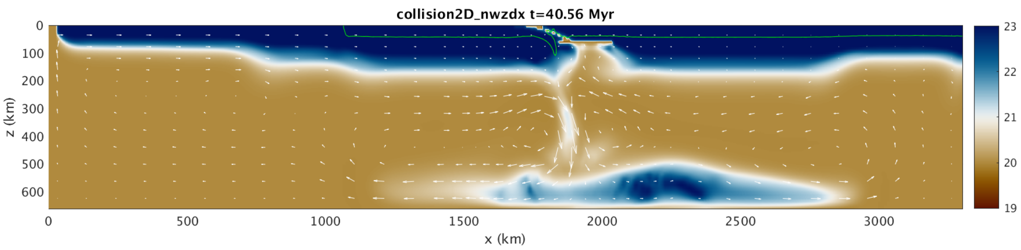
collision2D_nwzdx t=40.56 Myr
z (km)
x (km)
0 100 200 300 400 500 600
0 500 1000 1500 2000 2500 3000
19 20 21 22 23

(e)

Figure 3.1: Time evolution of the subduction process for the reference model. I am here representing the viscosity field. The color bar indicates the order of magnitude of the viscosity (in Pa s), while the blue area identifies the lithosphere (both continental and oceanic, which have the same viscosity) and the beige area the mantle. The green contour represents the continental crust, and the white arrows the velocity field. In figure (a) is represented the initial setup of the subduction process. Figure (b) shows the moment in which the slab reaches the lower boundary. Figure (c) identifies the necking of the slab. Figure (d) corresponds to a time immediately after the slab break-off. Figure (e) represents the end of subduction.

As discussed in chapter 2, in this model the passive margin is not taken into account and we considered the following values for the parameters:

- Crustal thickness: $h_c = 40$ km
- Crustal density: $\Delta\rho_c = 600$ kg/m^3

Slab break-off occurs (between 14and24 Myr) and at a depth of about 236 km and the continental crust reaches 150 km.

3.1.1 Changing the parameters of the crust

In most of the models presented in this study slab break-off does occur. However, there are a few end-member cases in which this does not happen. If I change the values of crustal density and thickness, by making the continent overall less buoyant, I reach a point in which the slab does not break-off. One of such cases is presented in figure 3.2.

Here, I chose the following values for the crustal parameters:

- Crustal thickness: $h_c = 30$ km;
- Crustal thickness: $\Delta\rho_c = 400$ kg/m^3.

The figure shows that the break-off does not occur and the continental crust continues to subduct into the upper mantle.

3.2 Passive margins with a ramp-type geometry

The geometry type whose time evolution is presented in figure 3.3 is the one described in figure 2.5.

In this model I chose the following values for the parameters:

- Crustal thickness: $h_c = 40$ km;

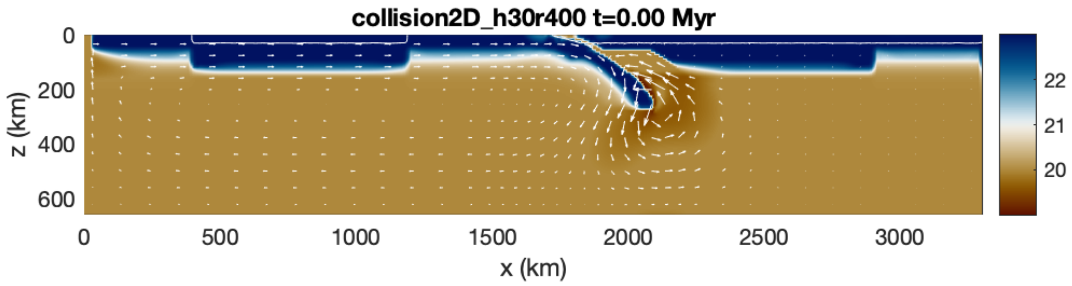

(a)

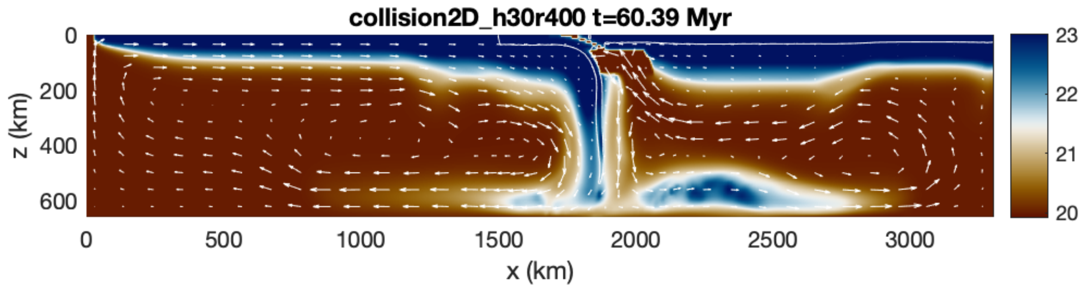

(b)

Figure 3.2: (3.2a) Setup and (3.2b) slab break-off for a model similar to the reference one. The colours indicate the logarithm of viscosity (with unit Pa s).

- Crustal thickness: $\Delta\rho_c = 500$ kg/m^3;

- Final thickness of the margin: $h_m = 20$ km;

- Margin length: $l_m = 50$ km.

First of all, I noticed that slab break-off does occur and it takes place later than in the reference model. Here, in fact, slab break-off happens at about 25 Myr, and at a depth of about 250 km. In this case, therefore, adding a passive margin with a ramp-type geometry slows the subduction process down and slightly delays the break-off.

3.3 Adding an oceanic crust

The next step is to take into account the presence of oceanic crust. I chose to maintain the same geometry as in section 3.2, with a crustal thickness of 30 km, and to add an oceanic crust with a ramp-type geometry. The oceanic crust goes from a thickness of 20 km to 7 km, has a density of $\Delta\rho = 300$kg/m^2, and it maintains the latter value until it reaches a depth of about 40 km, where it undergoes a phase transitions from basalt to eclogite (*Hacker, 1996 [33]*). After this transition, its density is the same as the density of the mantle.

The process is described by figure 3.4.

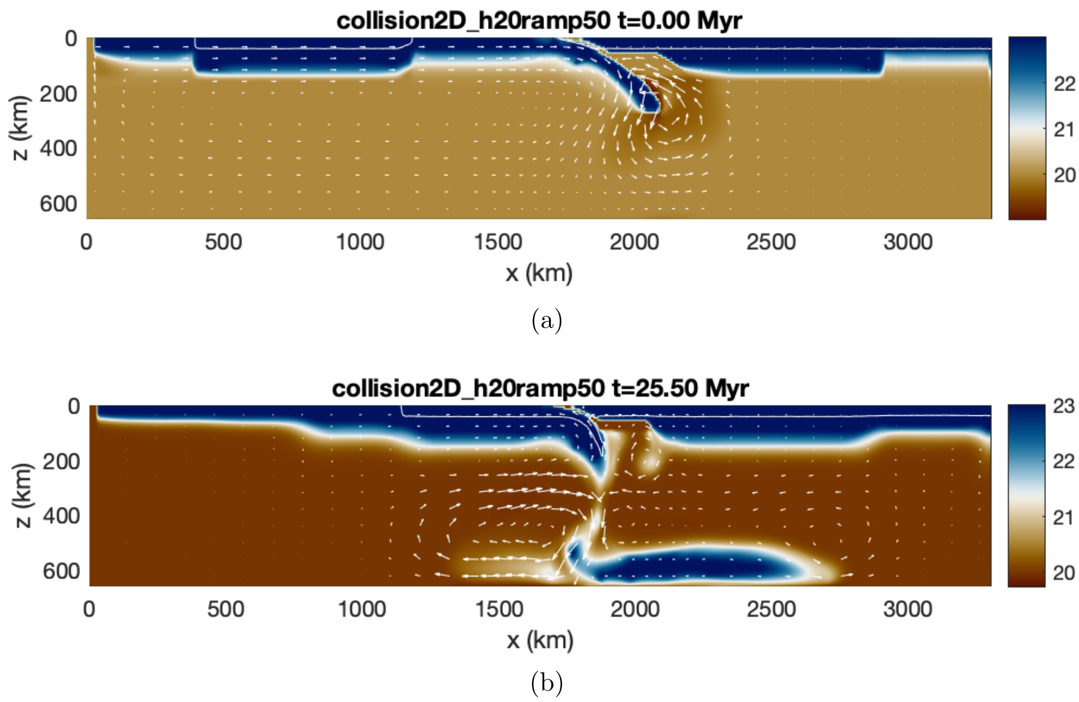

Figure 3.3: (3.3a) Setup and (3.3b) slab break-off for a margin with a ramp-type geometry. The colours indicate the logarithm of viscosity (with unit Pa s).

As it can be noticed, the break-off occurs at about 22 Myr and at a depth of about 370 km, which is faster than the previous models. This may be due to the fact that the oceanic crust, whose buoyancy is lower than the one of the continental crust, pulls the slab into the mantle and the process accelerates.

3.4 Magma Poor margins

Magma poor margins are described in figure 2.7. As discussed in section 2.3.4, they are characterized by a weak rheology and a long ramp-type margin. The crustal thickness in this model is 30 km.

The model represented in figure 3.5 corresponds to a margin with length 500 km and viscosity 10^{21} Pa s, which is two orders of magnitude lower than the rest of the crust. In the magma poor models, the oceanic crust is not taken into account.

The first thing that can be noticed is that the slab break-off occurs at about 56 Myr. Another interesting feature is that part of the margin does not subduct, but, instead, is accreted on the overriding plate. This two characteristics are present in all the magma poor models, and will be discussed in Chapter **??**.

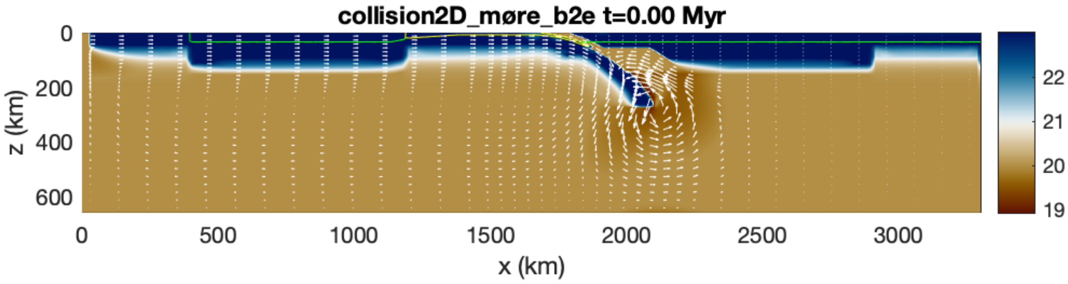

(a)

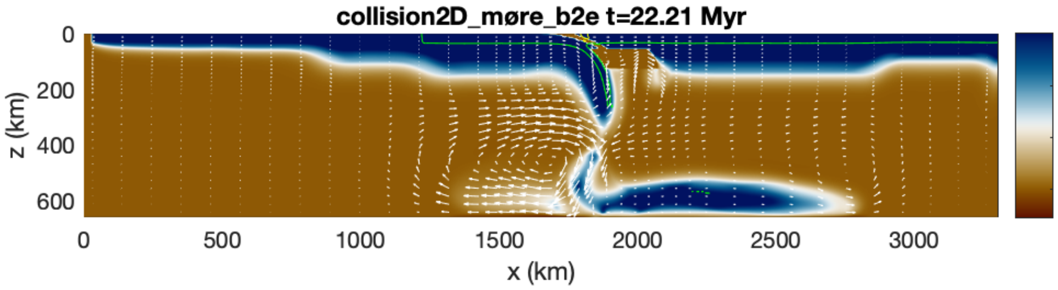

(b)

Figure 3.4: Setup and slab break-off for a margin with a ramp-type geometry and an where the oceanic crust is taken into account. The colours indicate the logarithm of viscosity (with unit Pa s).

3.5 Magma Rich margins

The schematic representation for the magma rich model outlined in figure 3.6 is the one in figure 2.8.

Magma rich margins are characterized by a thicker-than-normal oceanic crust, which we modeled as described in section 3.3, and a lower crustal body which coincides with a high velocity zone (HVZ) for the seismic waves (see Chapther 2).

I chose the following values for this model:

- Crustal thickness: $h_c = 40$ km;
- Length of the continental part of the margin: $l_m = 50$ km;
- Continental crust density: $\Delta\rho_c = 500$ kg/m^3;
- Oceanic crust density: $\Delta\rho_o = 300$ kg/m^3;
- Lower crustal body density: $\Delta\rho_{HVZ} = -100$ kg/m^3;
- Lower crustal body viscosity: $\eta_{HVZ} = 10^{24}$ Pa s.

I notice that the break-off occurs at about 44 Myr (the process is faster than for the magma poor margins) and that it occurs above the lower crustal body, which completely subducts into the upper mantle. This may be due to the high density of the HVZ, which highly reduces its buoyancy.

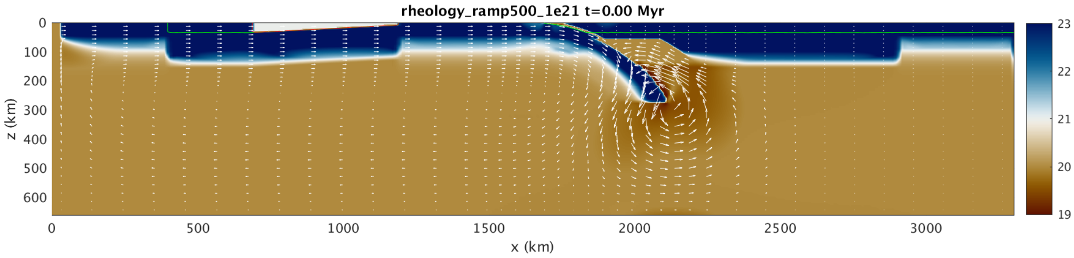

(a)

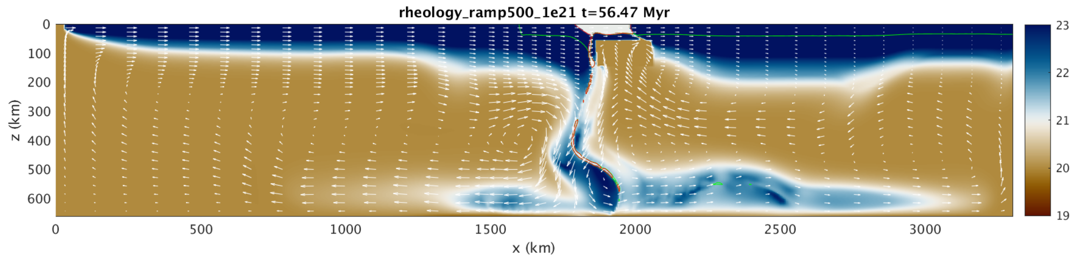

(b)

Figure 3.5: Setup and slab break-off for a magma poor margin. The green contour identifies the continental crust and the red contour identifies the passive margin. The colours indicate the logarithm of viscosity (with unit Pa s).

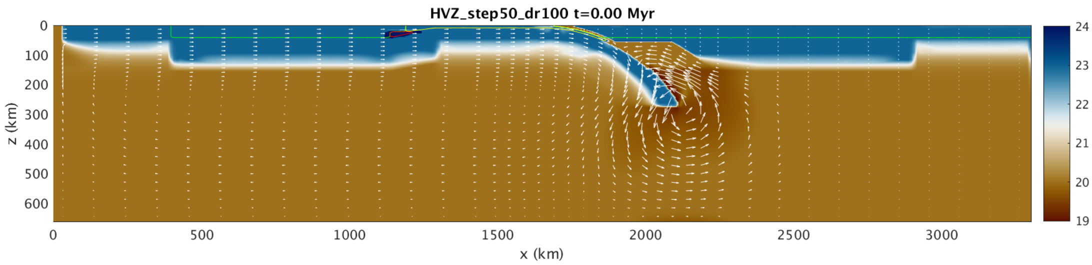

(a)

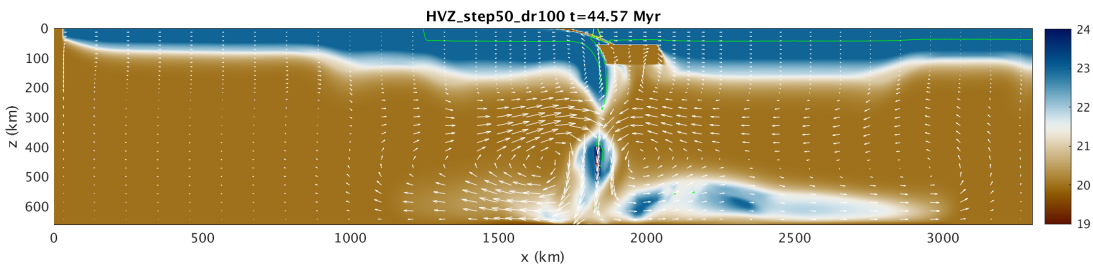

(b)

Figure 3.6: Setup and slab break-off for a magma rich margin. The colours indicate the logarithm of viscosity (with unit Pa s).

Chapter 4

Models Comparison

In the previous Chapter, a description of the geometries and rheologies implemented in Citcom has been presented, along with a report of the results of the main models of each group, individually.

The main goal of this Chapter is to compare the models in order to understand if any trend can be observed when we change the geometry of the passive margin, the density contrast between the continental crust and the ocean, and the rheology. In particular, I look at the break-off time and break-off depth of the slab as a function of the varying parameters, as well as what happens to the margin material throughout the process, to study the differences in the subduction evolution of each model after continental collision.

Here, therefore, the observations arose from this analysis are presented.

4.1 Comparison between all the models

Some preliminary observations can be made by comparing all the models of this study, and looking at the slab break-off depth and time as a function of the product between the density contrast and the thickness of the continental crust. This quantity describes the 'buoyancy contrast' between the passive margin and the rest of the subducting plate. Thus, the smaller the values of the buoyancy contrast, the denser the passive margin is. This gives an idea of the effect that the buoyancy of the passive margin has on the subduction dynamics. This kind of plot allows me to identify a depth and time range in which slab break-off occurs in the studied parameter space and, importantly, it gives a clear view of the impact that the geometry and density change have with respect to the rheology.

This can be observed in figure 4.1, in which the two main groups of models (geometry, described in sections 2.5.1, 2.5.2, 2.5.3; rheology, described in sections 2.5.4, 2.5.5) we implemented can be recognized, thanks to the different markers. A trend can be immediately identified: when the "buoyancy contrast" increases (the x-axis represents the product between density contrast and the thickness of the continental crust, so we don't have information about the buoyancy here, but about the buoyancy contrast), both the break-off time and the break-off depth decrease, following a linear law. This means that if the buoyancy of the continental crust increases (i.e. the crust is less dense), slab break-off happens earlier in time and at shallower depths. The decrease in buoyancy, thus, slows down the process and allows the continental part of the slab to reach larger depths in the upper mantle before the break-off. Moreover, the time interval over which the slab break-off occurs is larger for the models in which the rheology changes than for the ones in which we only take into account geometry and density changes. By looking at figure 4.1, in fact, we can see that the range of the slab break-off times goes from about 10 Myr to about 60 Myr for the models in which we modified the rheology of the passive margin, while the range for the models considering just geometry or density changes goes from about 10 Myr to 45 Myr.

In general, however, there is high variability even within each one of the two groups, even when we consider just the geometry and density changes. This means that all the parameters we considered in this study are important, because they clearly affect the timing and location of slab break-off. All this parameters together, in fact, define the architecture of the margin The values of the variability ranges and their detailed description can be found in the following sections.

I also investigate how long it takes for slab break-off to happen after the onset of collision as a function of the contrast buoyancy. Results are shown in figure 4.2, and this new break-off time is represented by the variable ΔT.

It can be noticed that the trend for this new quantity indicates that when the buoyancy contrast decreases, ΔT decreases following a linear law. This behaviour reflects the one found when considering the break-off time independently from the collision time. For simplicity and because this is a more meaningful value that can be compared to natural examples, from now on, we will show the break-off time always with respect to the onset of collision (ΔT).

4.2 Geometry and density changes

In this section, I compare the models in which I changed the geometry and the density of the margin. This first approach enabled me to have a first understanding of some of the margins spread throughout our planet, as well as give us a basis to start building models able to describe magma poor and magma rich margins. I conducted mainly parametric studies to investigate the different model evolutions by starting with simple passive margin geometries and increasingly complicating them to better simulate the real examples of passive margins, the only exception

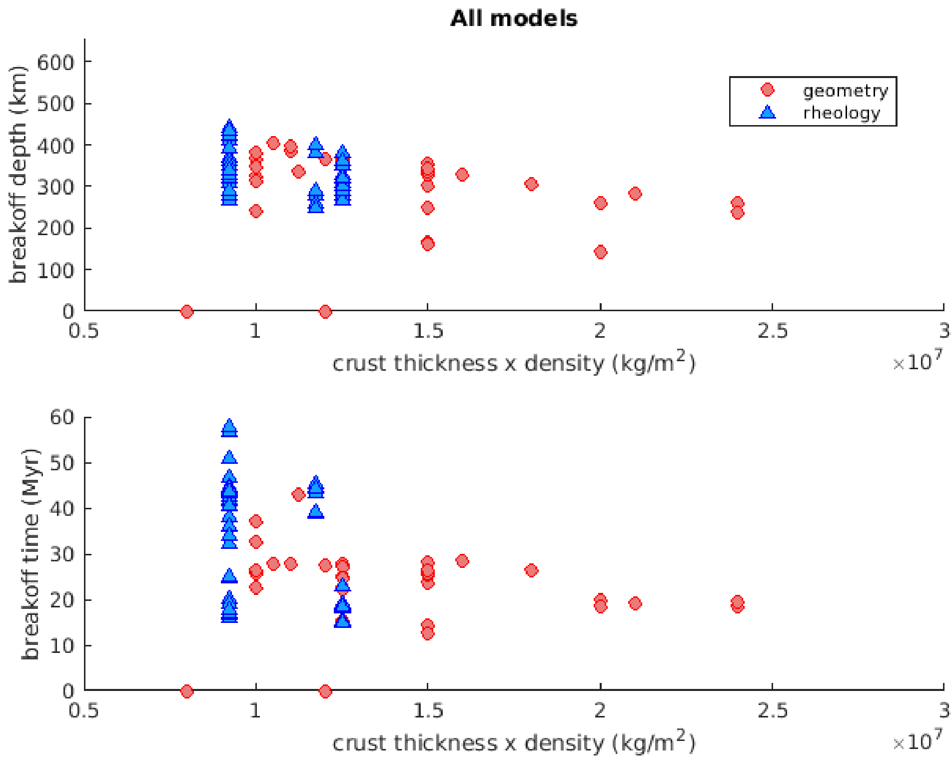

Figure 4.1: Slab break-off depth and time as a function of the buoyancy contrast of the continental crust.
The two groups represented in this figure and labeled "geometry" (red dots) and "rheology" (blue triangles) in the legend represent, respectively, the models in which we changed the geometry and the rheology of the passive margin, with different values of the buoyancy contrast. The points with value 0 km and 0 Myr for the break-off time depict the two cases in which no break-off occurred.

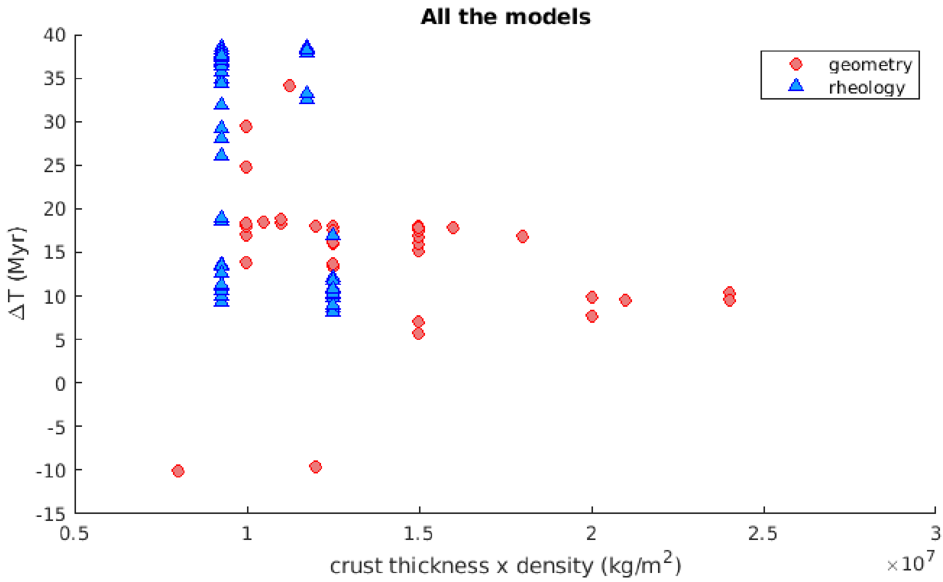

Figure 4.2: Slab break-off time with respect to the collision time as a function of the buoyancy contrast of the continental crust.
(see caption of figure 4.1 for details on the symbols)

being the group of models (described in section 4.2.3) in which I modeled real conjugate margins on Earth [19].

4.2.1 Reference models: abrupt transition between continental and oceanic lithosphere

As described in paragraph 2.4, I started with a set of models with no passive margin, which means that a sharp transition between continental and oceanic lithosphere is present. This case is a starting point, which will enable me to discuss the differences that arise when a passive margin is taken into account.

I vary the continental crust thickness from 30 to 40 km and the density contrast of the continental crust between 400 and 600 kg/m^3.

In this set of models, the break-off depths range between 260 km and 354 km and the ΔT between 9.43 Myr and 18.01 Myr (figure 4.3). When identifying these ranges I are not considering the model for which the break-off does not occur ($\Delta\rho$ = 400 kg/m^3; crustal thickness h = 30 km). Looking at figure 4.3 I can still recognize the same trend seen in figure 4.1, together with some more information.

First of all, I notice that if both the density contrast and the crustal thickness are small(the values of the passive magin density contrast is either 400 kg/m^3, 500 kg/meter^3 or 600 kg/m^3, while the crustal thickness values are 30 km, 35 km or 40 km), slab break-off does not occur, and the continental crust is completely subducted. However, this is an end-member case. Indeed, if I increase the value of the crustal thickness to 40 km without changing the value of the density, slab

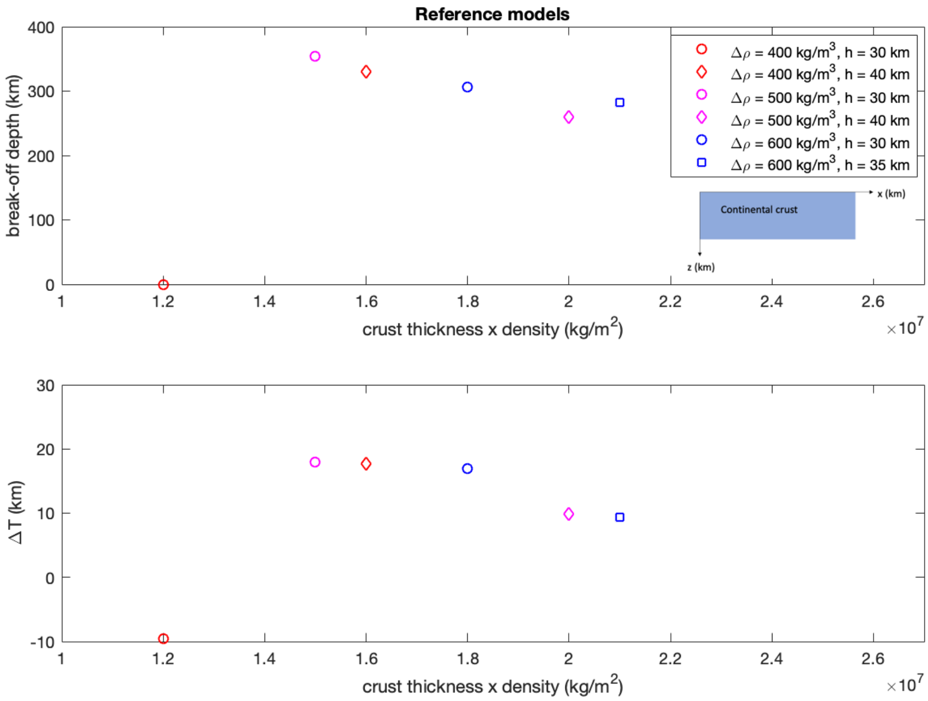

Figure 4.3: Slab break-off depth and time as a function of the buoyancy contrast of the continental crust for the models in which the passive margin is not taken into account. The markers colour represents the value of the density contrast, which is reported by the colour-bar on the right. Their size represents the crustal thickness: the bigger the marker, the thicker the continental crust is.

break-off occurs.

I observe that models with the same crustal density show a decrease in the value of both the break-off depth (from 354 to 236 km) and time (from 28.26 to 19.13 Myr) if the crustal thickness increases.

4.2.2 Passive margins with a ramp-type geometry of variable length and height

In this second set of models, I take into account the presence of a transition zone between the ocean and the continent, i.e. the presence of a passive margin. I start with a simple geometry of a ramp of variable length and thickness.

I therefore compare these models by looking at the break-off time and depth as a function of the ramp length, as shown in figure 4.4.

The results show that the range of slab break-off depth and ΔT are, respectively, from 301 km to 367 km and from 16.03 Myr to 29.45 Myr. I are therefore considering a depth variation of 66 km out of 660 km (which is the depth of the box) and a time variation of about 13 Myr.

The results in the first plot of figure 4.4 show that when the ramp height is

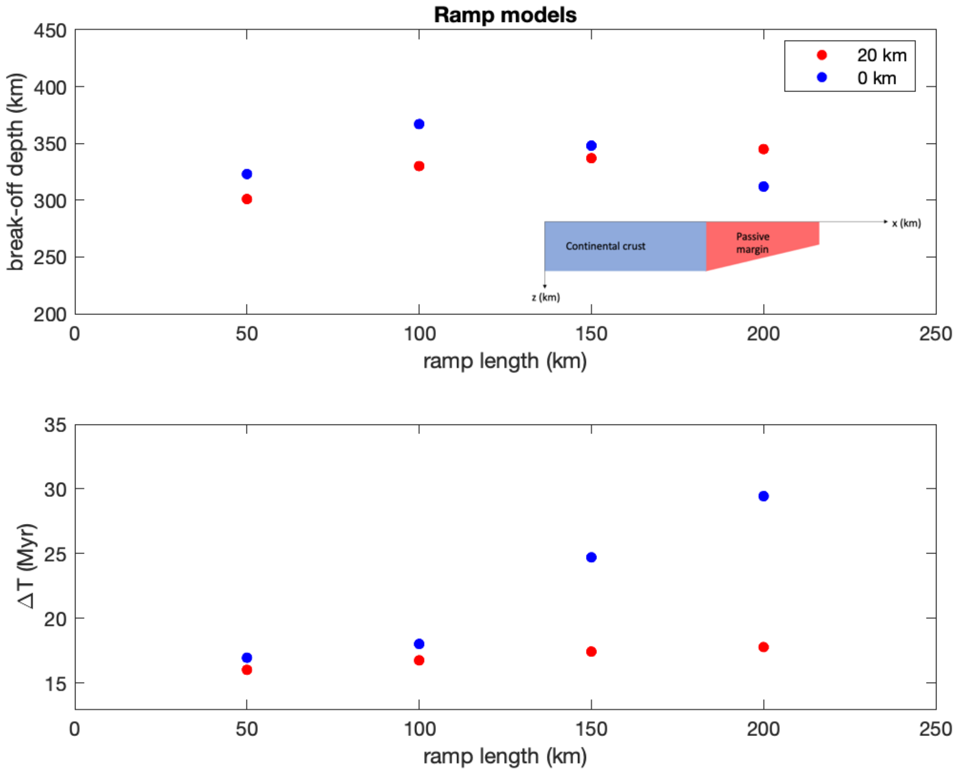

Figure 4.4: Break-off depth and time as a function of the ramp length of the passive margin for the ramp models. The colour of the markers identify final values of the crustal thickness.

20 km, the slab break-off depth increases when the ramp length increases, while when the final crustal thickness is 0 km, the break-off depth increases up until the ramp length reaches 100 km, but when this value increases the break-off occur at shallower depths.

When it comes to the slab break-off time, I notice that for both of the values of the ramp height, the break-off time increases when the ramp length increases. However, while the increase for the case with ramp height 20 km is not very noticeable, when the ramp height is 0 km and the ramp length is bigger than 100 km, the increase has a much larger slope.

4.2.3 Passive margins on Earth: conjugate margins

In this group, I include all the models in which the geometries are based on real conjugate margins across the world, as described in *Peron-Pinvidic* [19].

Every margin is described by a different mathematical function: some as ramps (or series of ramps) of different length and height and some as trigonometrical functions (or series of trigonometrical functions).

I plotted the break-off time and depth as a function of the ramp/trigonometrical function length, taking into account the height of the ramp/trigonometrical function by choosing different sizes for the markers. The results are shown in figure 4.5.

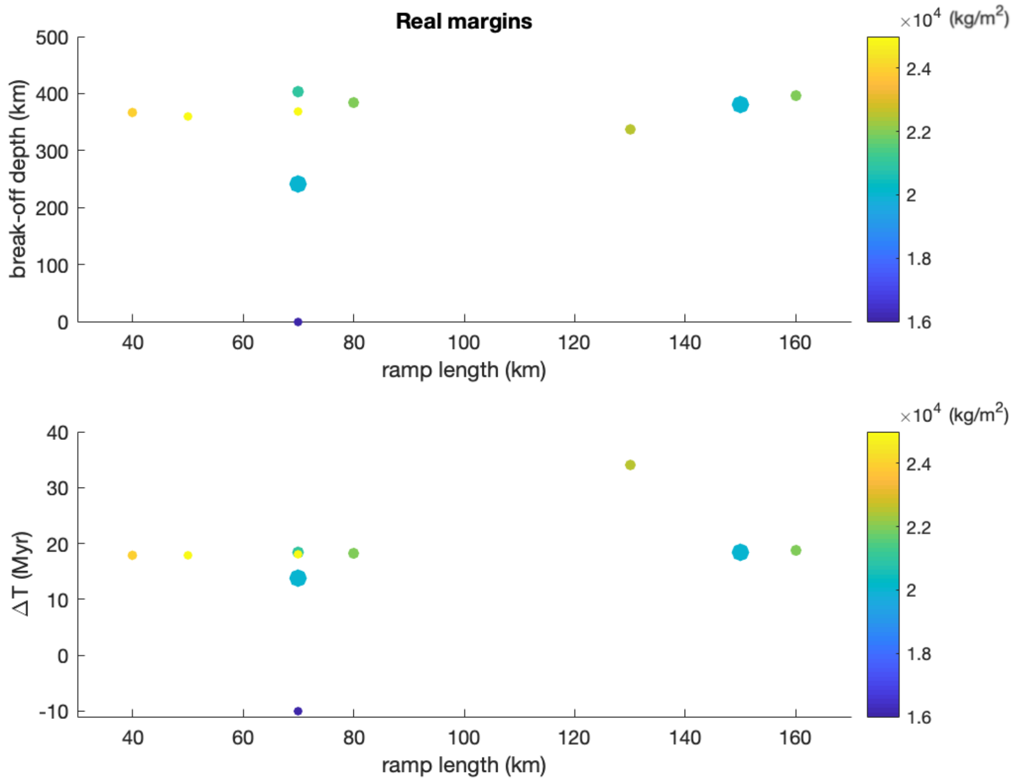

Figure 4.5: Break-off depth and time as a function of the ramp length of the passive margin for the real conjugate margins. The size of the markers identify different ramp heights (the shorter the marker, the smaller the value of the ramp height), while their colour refers to the buoyancy contrast, as indicated by the colour bar on the right side of the plot. In both plots, the value 0 identifies the case in which the break-off does not occur.

The results show that a trend is not easily identifiable when considering real margins, probably because when looking at more realistic geometries (i.e. when trying to replicate the characteristics of a specific margin) the slab break-off times and depths have more variability, since we are not conducting a parametric study.

In fact,when the break-off occurs, the time range goes from 13.79 Myr to 34.06 Myr, spanning about 20 Myr, and the break-off depth goes from 242 km to 403 km, spanning 161 km.

4.2.4 Adding an oceanic crust

Here I discuss the models in which an oceanic crust of variable thickness and geometry is added, in order to try and have a first distinction between magma-poor (very thin oceanic crust) and magma-rich (thicker than normal oceanic crust) passive margins.

I also included a model in which the oceanic crust is not taken into account and with the same passive margin's geometry. This choice was made in order to understand if adding an oceanic crust may change the subduction dynamics significantly.

I chose to model the oceanic crust as a block of thickness 0 km, 7 km, 20 km or as a ramp of average thickness 13.5 km.

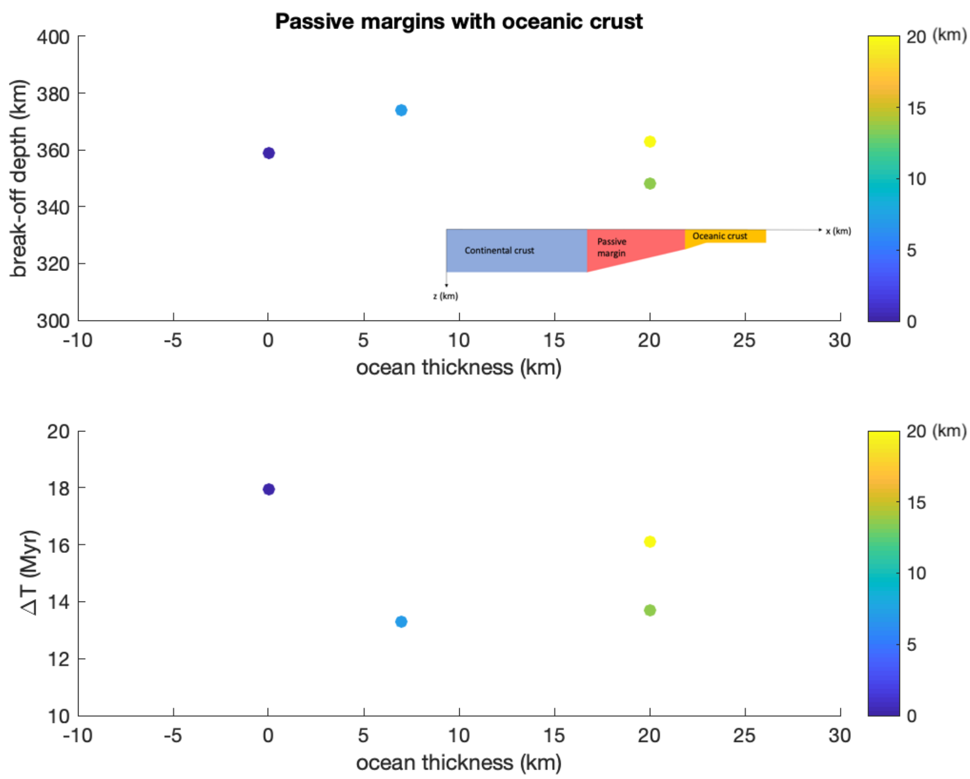

Figure 4.6: Break-off depth and time as a function of the initial oceanic crust thickness. The size of the markers identify the average oceanic crust thickness for every model.

The range of slab break-off depth is very small, going from 348 km to 374 km, as well as the time range that goes from 13.29 Myr to 17.93 Myr.

When looking at the slab break-off time plot, it can be noticed that the slab breaks at earlier stages of the subduction process when an oceanic crust is introduced, while there are no significant changes when it comes to the break-off depths (the values span 26 km.

4.3 Rheology changes

The two kinds of passive margins I took into account in this project are the magma poor and magma rich ones.

In this section, I present the results that arise from the comparison between different rheologies associated with the same type of margin, to see which are the main differences between these two groups and, within each one, what happens to the subduction process if I modify parametrically the rheology of the margin.

4.3.1 Magma Poor margins

In this section I present the results I obtained for magma poor passive margins, in terms of slab break-off.

Magma poor margins are characterized by a long (up to 500 km, if not more) transitional zone between the continent and the ocean composed of highly stretched and faulted continental lithosphere. Therefore, I considered this region to be weaker than the surrounding material.

I described these margins as ramps of variable length (from 100 to 500 km) and viscosity (from $5 \cdot 10^{20}$ to $5 \cdot 10^{22}$ Pa s).

The results are outlined in figure 4.7, where the break-off time and depth are plotted in function of the length of the ramp.

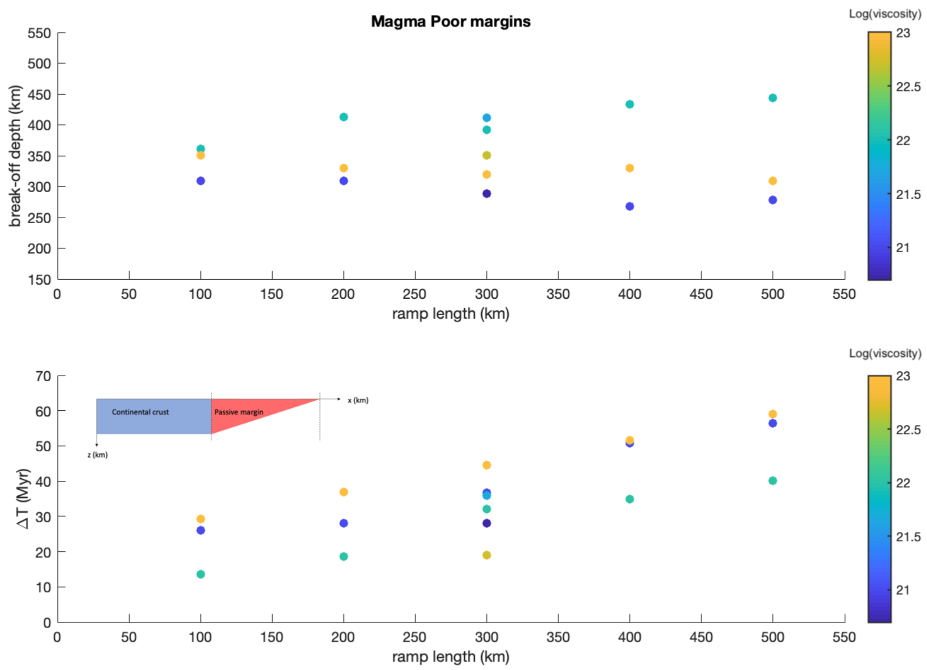

Figure 4.7: Break-off depth and time as a function of the ramp length for the magma poor models. The colour of the markers identify the order of magnitude of the passive margin's viscosity.

I notice that, for every single value of the viscosity, the break-off time increases with the length of the ramp. Furthermore, the variability is much higher than in the previous plots. For the slab break-off depth, however, it is more complicated to find a common trend. Indeed, I observe that the depth value increases with the ramp length for one of the values of the viscosity of the margin ($\eta_{MP} = 10^{22}$ Pa s) and decreases for all the other values (10^{21} Pa s, 10^{23} Pa s).

This had me believe that further investigations were necessary to describe the behaviour of these margins. The results are shown in the next Chapter.

4.3.2 Magma Rich margins

Magma rich margins have a shorter transition zone thank the magma poor ones and are composed of newly formed volcanic rocks: a thick layer of oceanic crust at the surface and, below it, a 'lower crustal body' that is likely to be the dense and strong residue of the volcanic products above it (*Stab et al.*, 2016 [32]).

I decided to describe these margins as ramps of length of either 50 or 100 km and viscosity 10^{24} Pa s. I also changed the density of either the whole passive margin or the lower crustal body. I chose the following values for the difference between the density of the margin and the one of the upper mantle: $\Delta\rho_m = 0; -100$ or -200 kg/m^3 .

These margins are also characterized by a thicker-than-normal oceanic crust (up to 30 km; *Geoffroy* [14])

Figure 4.8 shows the results for the break-off time and depth for magma rich margins. Every group represents one of the geometries (described in figure 4.9) that have been implemented for magma rich margins during this project.

For this type of margins, again, a common trend is not easily recognisable, apart from the fact that the heavier the margin is (i.e. the higher the value of $\Delta\rho_m$ is), the smaller both the time and depth span for the break-off are. The models describing the margin as a ramp whose viscosity is higher than the rest of the plate (the red ones in figure) have a significantly smaller amount of time for break-off to occur compared to the others. Furthermore, slab break-off occurs above the margin for all the models, except for the ones in which the difference between the density of the HVZ and the mantle is 0 kg/m^3.

Once again, therefore, further investigations seem necessary, and will be presented in the next Chapter.

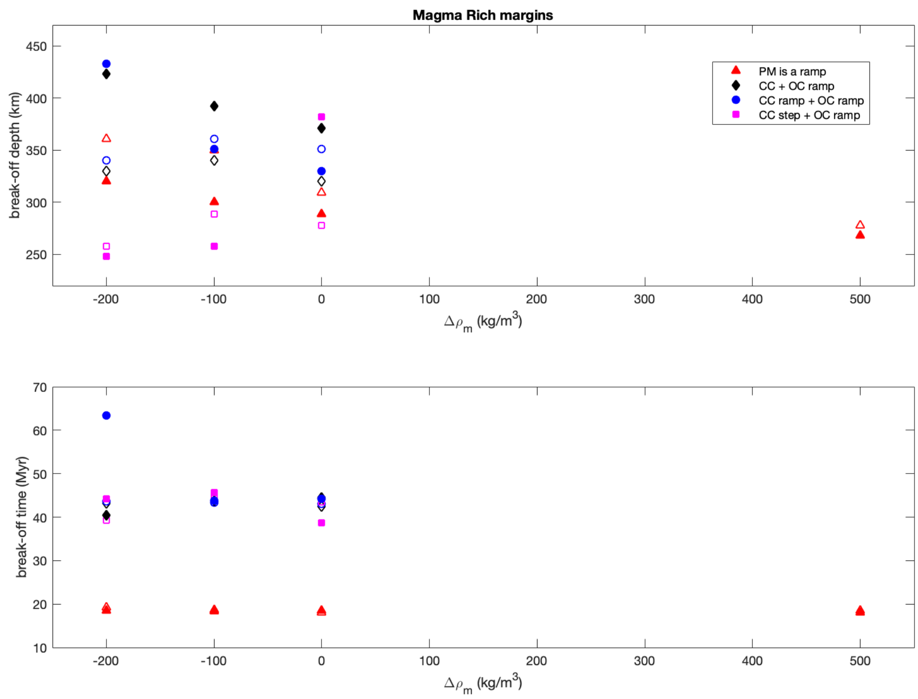

Figure 4.8: Break-off depth and time as a function of $\Delta\rho_m$. The colour and shape of the markers identify the passive margin's geometry, as described in figure 4.9

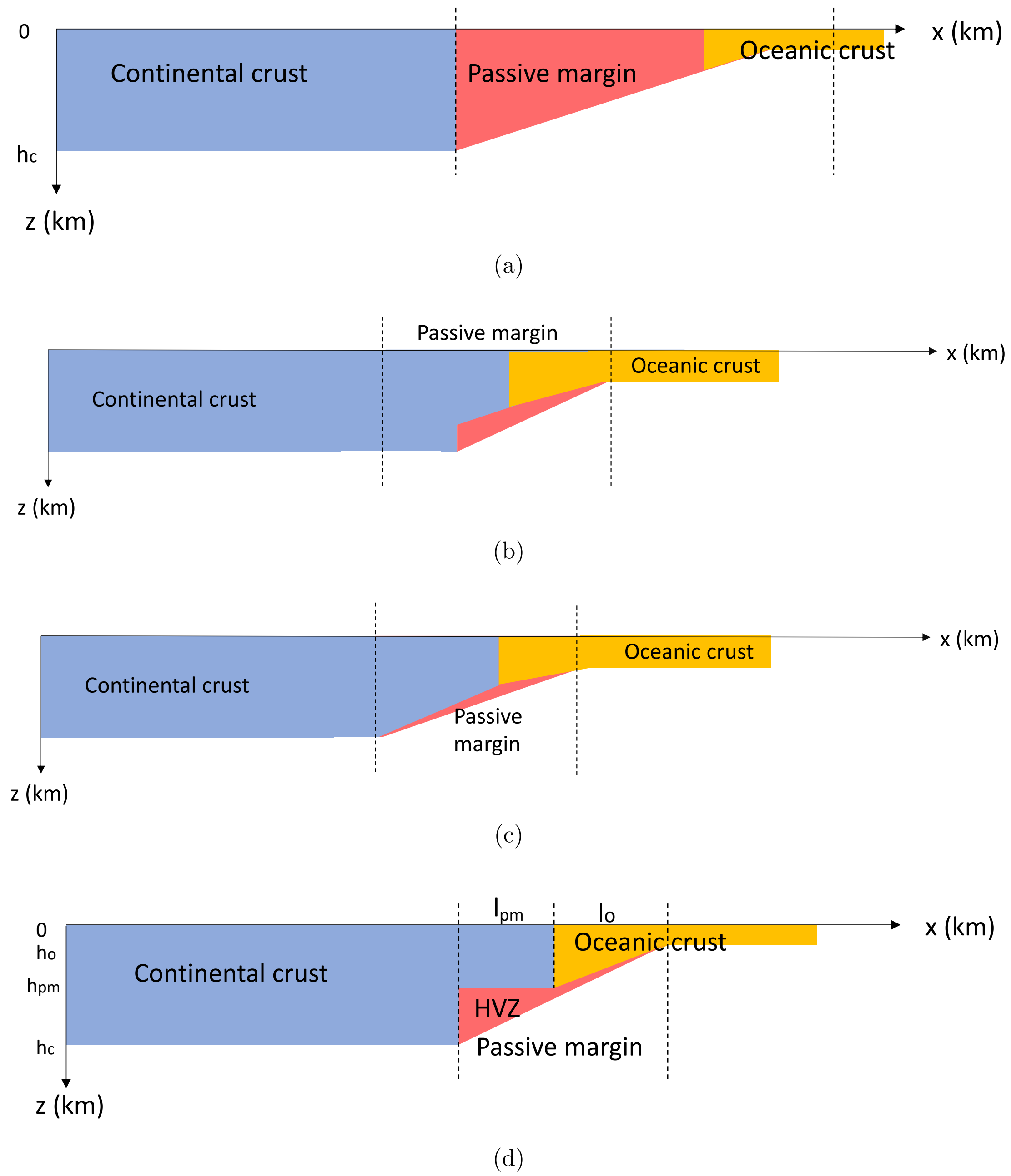

Figure 4.9: Types of magma rich margins we considered in figure 4.8: (4.9a) corresponds to the models labeled as a red triangle; (4.9b) to the ones labeled as a black diamond; (4.9c) to the ones labeled as a blue circle; (4.9d) to the ones labeled as a magenta square.

Chapter 5

Discussion

The aim of this Chapter is to discuss the results presented in Chapters 3 and 4. In particular, I will try to find an explanation for the trends and features I outlined. I will therefore discuss processes like the slab break-off for all the models, as well as some other features which are present just in some groups of models, like the accretion of margin material on the overriding plate in the case of magma poor margins.

All the considerations which will be presented in this Chapter arise from further processing of the data we obtained through my models using MATLAB, or from the comparison with other studies on subduction zones and passive margins (even if the literature in this latter case is not extensive). I will also try to explain some of the processes I encountered thanks to studies relative to natural cases, in order to understand if my models can actually be considered relevant with respect to geological features of our planet.

Furthermore, I will try to answer the question whether the rheology or the geometry of a margin has the more important effect over the subduction process.

5.1 Other studies on continental collision

Many numerical studies exist on the dynamics of continental collision and they show a wide range of values for slab break-off depth and time. *van Hunen et al.*, 2011 [7] modelled 2D subduction problems, with a continental block 40 km thick, with density 600 kg/m^3 and no passive margin. In their models, slab break-off occurs at 10 Myr (for young, weak slabs) to more than 20 Myr (for old, strong slabs), and it occurs deeper than 200 km. *Magni et al.*, 2012 [5] is the model I used as a starting point for this work, and it describes a model which is the same as the reference one in this study, except for the presence of a weak zone at the right boundary. In this case, slab break-off occurs at 17.2 Myr from the start of the computation. These values are in agreement with my results, however, when considering the presence of a more realistic passive margin, I obtain a wider range of values both in terms of slab break-off depth (300 km) and time (50 Myr). This shows that it is important to include passive margins in these type of models because they indeed affect the dynamics of continental collision. *Baumann et al.*, 2010 [8] describes a model in which the lower mantle is part of the domain. In this case, slab break-off happens at much higher depths ($410 - 510$ km) and at about $40 - 50$ Myr due to the buoyancy effects on the boundary. However, I did not consider the lower mantle in this work, so a comparison with this study is not possible.

5.2 Reference models: abrupt transition between continental and oceanic lithosphere

The results for this set of models, in which there is an abrupt transition between continent and ocean, are shown in sections 3.1 and 4.2.1.

I modified the thickness of the continental crust, as well as its density, to understand the role of the buoyancy in the subduction dynamics.

Figure 4.3 shows that when the value of the buoyancy contrast increases (and the buoyancy decreases), the depth and time of the slab break-off increase. This variation in time, however, is not extremely significant, since its value is of the order of 10 Myr. The variation in depth, on the other hand, spans about 100 km. This trends can be explained by the fact that the increase in buoyancy may prevent the crust to sink deeper into the mantle, counterbalancing the pull of the lithospheric lab which has already been subducted, and causing the slab break-off to happen at shallower depths and faster.

These estimates, however, do not include the case in which the break-off does not occur. Here, I am considering the situation described in figure 3.2. In this case, I modelled a very thin crust with high density. These two characteristics, combined, result in a continent that is heavy enough to subduct and maintain a ductile behaviour. This results in the complete subduction of the continental lithosphere without any slab break-off.

5.3 Passive margins with a ramp-type geometry of variable length and height

An example for this group of models is shown in section 3.2. Figure 4.4 shows the slab break-off time and depth in terms of the length of the passive margin. The final thickness of the margin is also taken into account thanks to the color of the markers in the plot.

As described in section 4.2.2, the geometry of the passive margin seems to significantly affect the subduction dynamics.

In fact, if I consider a margin with final thickness of 20 km, both the slab break-off time and depth increase steadily with the margin length. This may be due to the fact that the longer the margin is, the thinner it becomes after the subduction. This may be due to the overall buoyancy: since the crustal layer (which is lighter because the density of the crust is lower than the one of the mantle one) is thinner for a more extended part of the margin, it takes longer to subduct enough light material (i.e., the continental crust) to produce enough stresses to break the slab at depth.

On the other end, if the final thickness is 0 km, the slab break-off depth increases if the margin length is 50 or 100 km, and then it decreases. The break-off time, in this case, increases more rapidly for a margin of length larger than 100 km. This may due to the fact that the margin changes shape during the evolution, and it becomes similar to the case in which the margin is not taken into account. This means that we have thicker crust that does not subduct as much as in the previous cases, causes slab break-off to occur at shallower depths but delayed in time.

5.4 Adding an oceanic crust

The evolution of this group of models is outlined in section 3.3, and a comparison in terms of initial and average thickness of the oceanic crust can be found in figure 4.6.

For all the models, slab break-off happens at shallower depths and later in time when the oceanic crust is not taken into account. In general, though, there are no significant differences, because the break-off time and depth variations are not very large. This may be due to the transition from basalt to eclogite at a depth of approximately 40 km, which confines the effect of the oceanic crustal buoyancy only close to the surface. Its role in the subduction dynamics is, therefore, limited.

5.5 Magma Poor margins

An example for magma poor margins may be found in section 3.4, and a study of the slab break-off in terms of the margin length and viscosity is presented in figure 4.7.

The break-off time increases steadily with the margin length for all cases, but I do not see a consistent behaviour in terms of the viscosity. Furthermore, the break-off depth does not show an identifiable trend both for the margin length and viscosity, as described in section 4.3.1.

In order to understand better this behaviour, I chose to consider a margin with length 300 km, and vary the viscosity in a systematic way from 5×10^{21} Pa s to 10^{23} Pa s. What I expect, is that when the viscosity decreases, the margin breaks more easily because it becomes weaker. What I see, however, is what follows:

- Break-off depth: The slab breaks at shallow depths for the lowest value of the viscosity, then it happens deeper for the value half an order of magnitude larger, and then decreases again;
- Break-off time: There is no discernible trend.

This kind of behaviour may be due to the fact that my models show (figure 3.5) that not all the margin is subducted, but part of its material is accreted on the overriding plate.

The percentage of material that remains in the first 40 km of the domain along the z-axis, and is eventually accreted is shown in figure 5.1. This figure shows how much material of the passive margin stays at the surface during the model evolution and the final values towards the end of the curve show how much material is accreted to the overriding plate once continental collision is over.

A description of the models considered in this figure (in terms of the parameters I used to model them) can be found in table A.5 in appendix A. Figures that show the accreted and subducted margin material for magma poor models as a function of their viscosity and margin length can be found in appendix B.

The cause for the high variability in behavior for the break-off in magma poor margins may be the buoyancy: the slab loses the light part, which stays at the surface, thus it remains heavy for longer. The weakness of the passive margin is very important to allow the decoupling between the passive margin material and the lithosphere below. As shown in previous models with no weak passive margin, this type of decoupling would not happen otherwise.

Furthermore, the longer the ramp, the more material is exhumed and accreted on the overriding plate, as shown in figure 5.2.

This feature I found in our models is consistent with geological measurements which show that magma poor margin material can be found in mountain ranges such as the Alps (*Manatschal and Gianreto*, 2004 [18]).

5.6 Magma Rich margins

The time evolution of magma rich margins can be found in section 3.5 and a comparison in terms of type of model and density of the HVZ can be found in

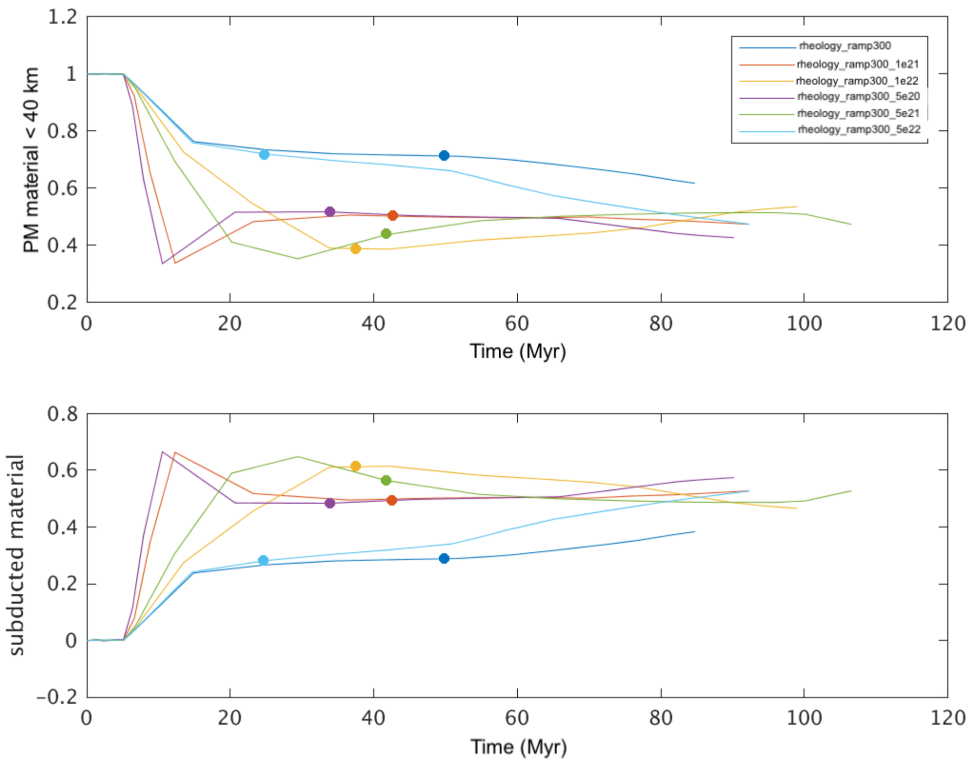

Figure 5.1: Magma poor margin material which is subducted and, at the end of the process, accreted on the overriding plate for a margin of length 300 km and variable viscosity. Figure (a) shows the margin material that remains in the first 40 km of the domain along the z-axis, which becomes accreted material at the end of the process. The break-off time is represented by the dots. Notice that after the break-off, part of the margin material is exhumed.

figure 4.8.

In general, the depth of the slab break-off seems to decrease when the density of the lower crustal body decreases. This can be due to the fact that an increase in density causes a decrease in the buoyancy, and this allows the slab to sink further into the mantle. The break-off time, however, does not show any noticeable trend.

Looking at figure 3.6, however, it can be noticed that the slab breaks above the margin. This happens in most of our models, except for the ones in which the HVZ has the same density as the mantle. In these cases, the passive margin material is exhumed. Importantly, the occurrence of slab break-off within the subducting continent and above the passive margin material, means that the passive margin is "lost" into the mantle and does not exhume. It is, thus, hard to preserve magma rich passive margins due to their properties. This behaviour is consistent with the fact that magma rich margins are not as common as magma poor ones on Earth. In fact, if they are subducted in most of the cases, they cannot be seen on the surface. An exception to this feature can be found in the Møre Basin in Norway

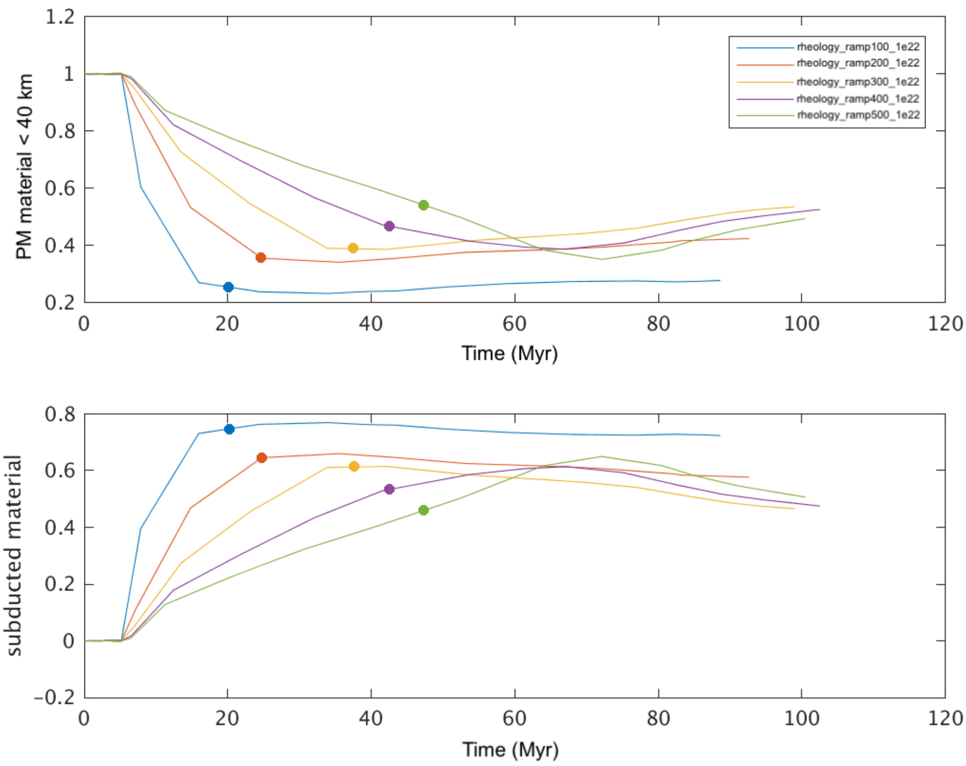

Figure 5.2: Magma poor margin material which is subducted and, at the end of the process, accreted on the overriding plate for a margin of viscosity 10^{22}Pa s and variable length. Figure (a) shows the margin material that remains in the first 40 km of the domain along the z-axis, which becomes accreted material at the end of the process. The break-off time is represented by the dots.Notice that after the break-off, part of the margin material is exhumed.

(*Jakob et al.*, 2019 [34]), which is a fossil magma rich margin.

5.7 Geometry or rheology?

Since the ranges of time and depth vary significantly with the different models, I asked myself whether the geometry or the rheology of the margin has the more critical impact on the subduction dynamics.

Figure 4.1 shows an overview of the slab break-off time and depth for all the models I studied. By looking at this plot I observe that, at least for the break-off time, the rheology seems to be the main factor in terms of the variation of the time evolution of the system. When looking at the depth, however, the geometry seems to be the most important feature.

However, when considering the rheology, I considered a smaller number of different geometries for my models. This leads me to think that if I were to perform all the rheology changes I discussed for every geometry I built, I would see that the slab break-off depth variations would be regulated by the rheology as well.

In general, both rheology and geometry are very important when modelling passive margins. In fact, they both show high variability in terms of slab break-off, and the variability is more evident in the cases in which I consider both of these features (i.e. we change the architecture of the margin), for example in magma rich margins.

The models in which I considered the real margins on earth, moreover, show that I can obtain a significant variability for the subduction process if I just consider the geometry changes.

Therefore, even if geometry is definitely a key factor when considering the effect of passive margins on subduction, I believe the rheology to be the main element that has to be taken into account when trying to understand how passive margins affect the continental collision dynamics.

5.8 Models limitations

All of the models I studied in this work present some limitations and could be expanded in order to describe margins which approximate better real cases.

First of all, I considered 2D models, and this does not give me any information about how the dynamics changes if we consider a plate which has a finite extension on the horizontal plane. I also considered the domain to stop at the base of the upper mantle, but in some cases, the slab sinks into the lower mantle as well. This may also be interesting if I want to try and reproduce natural cases.

Moreover, when introducing the rheology changes, we assigned a fixed value of the rheology to the margins, without taking into account the fact that the viscosity is not constant but does, in fact, change during the subduction process. In order to describe more realistic cases, therefore, a variable viscosity may be introduced, for example as a function of the temperature and stresses. We are, therefore, considering passive margins, but they are much simpler than the real cases.

Another feature I haven't considered here is that passive margins, especially magma poor ones, are usually covered by a thick sediment layer, which present a weak rheology. When I modeled MP passive margins, I considered them to be weaker than the rest, but since the sediment layer is just a few kilometers thick, I can not consider it to represent the whole margin, so I cannot include it in the rheology we chose for this type of margins.

Furthermore, magma rich margins present a lower crustal body, corresponding to a high velocity zone for seismic waves. In all of my MR models, I considered this HVZ to be stronger than the rest. This fact, however, is uncertain. It is still not clear, in fact, what this body is [32], and we assumed it is mafic/ultramafic material that is stronger and denser than the surrounding material. I tested different values for the viscosity and density parameters and the results did not change significantly. The margin, in fact, always subducted. However if this body and, in general, the whole margin is serpertinized and/or highly faulted, then its rheology can change and the margin could be overall weaker. Further studies could therefore be done to address this problem, in order to understand if the rheology of the HVZ might affect the subduction dynamics significantly.

Chapter 6

Conclusions

The aim of this work was to understand different types of passive margins can influence the dynamics of continental collision. The subduction process has been modelled using the finite element code Citcom and to describe the dynamics of continental collision I mainly focused on the time and position of the slab break-off after the collision and on the fate of the passive margin material.

I decided to focus on the two main types of passive margins existing in nature, which are the Magma Poor and Magma Rich ones. They differ from one another because of the processes that originated them. Magma Rich margins are associated with heavy magmatism during their formation. This creates a thicker-than-normal oceanic crust and, below it, the presence of a lower crustal body, which it thought to be the residue of the effusive magmatic material above and is identified as a high velocity zone for the seismic waves. Therefore, this lower crustal body is assumed to be an area with viscosity and density higher than the rest of the crust. Magma Poor margins are described as transitional zones between continent and ocean whose length can reach and exceed 500 km, and are heavily stretched and faulted areas. In my models, I assigned them a lower viscosity than the rest of the crust. A schematic representation of these margins can be found in figures 2.8 and 2.7.

To model these margins, I started by introducing in the model described in *Magni et al.* [5] passive margins with the same rheology as the continental crust but with different geometries. Afterwards, I changed their density, in order to understand the role of buoyancy in the subduction dynamics, and, in a few cases, I introduced an oceanic crust, to start identifying the role of a thicker-than-normal oceanic crust. Finally, I introduced some rheology changes that allowed me to discriminate between magma poor and magma rich margins. In total, I obtained 92 models. The main ones are described in Chapter 3.

I compared these models as a function of the varied parameters (e.g., geometry parameters, density, and viscosity), in order to understand what exactly is the effect of passive margins on subduction and if it is actually important to consider them when modelling this phenomenon. This comparisons and the discussion of the results are outlined in Chapters 4 and 5. In general, it can be noticed that passive margins certainly have a noticeable impact on subduction, especially when it comes to slab break-off and the fate of the margin material throughout the process. The break-off time and position, in fact, change in a range spanning 50 Myr and 300 km, respectively. Furthermore, the factor that shows the higher impact on the subduction dynamics is the rheology of the passive margin. Magma poor and magma rich margins, in fact, behave quite differently from one another.The geometry and density changes, however, cannot be neglected as a key element when trying to understand how the presence of a passive margin affects subduction, since they still cause a wide variability range for the slab break-off. The results also showed that for magma poor margins part of the margin does not subduct but it, in fact, exhumes and accretes on the overriding plate. This is consistent with geological observations which show that magma poor passive margin material can be found in mountain ranges and is, thus, easily preserved. On the other hand, in most cases magma rich margins are completely subducted and lost into the mantle, because the slab breaks above them. This is consistent with the fact that fossilised magma rich margins in orogenies are much less common than the magma poor ones in nature.

This study, therefore, showed that passive margins are, in fact, important when modelling subduction and should be taken into account when studying this process because their structures controls the dynamics and timing of slab break-off and the accretion of passive margin material. Importantly, I provide an explanation on why it is easier to find accreted magma poor passive margins in mountain belts than magma rich ones.

Appendix A

Complete list of models

I present here the complete list of the models implemented in this project, divided in groups to highlight the main parameters we considered.

Abrupt COT					
Model name	**Margin geometry**	**Continent thickness** (km)	**Continent density** (kg/m^3)	**Break-off depth** (km)	**Break-off time** (Myr)
`collision2D_nwzdx`	-	40	600	236	19.6
`collision2D_drho500`	-	40	500	260	19.73
`collision2D_drho400`	-	40	400	330	28.28
`collision2D_cc35`	-	35	600	283	19.13
`collision2D_cc30`	-	30	600	306	26.25
`collision2D_h30r500`	-	30	500	354	28.26
`collision2D_h30r400`	-	30	400	-	-
`collision2D_h40step`	step function	40	500	141	18.38
`collision2D_step`	step function	30	500	248	23.49

Table A.1: These models represent an abrupt COT. Here, the passive margin is not present at all or it is represented as a step function.

Ramp-type geometry						
Model name	**Margin geometry**	**Average continent thickness** (km)	**Margin length** (km)	**Ramp height** (km)	**Break-off depth** (km)	**Break-off time** (Myr)
`collision2D_gradcc`	ramp	30	800	20	165	14.46
`collision2D_gradual`	ramp	30	800	20	160	12.62
`collision2D_h20ramp50`	ramp	30	50	20	301	25.5
`collision2D_h20ramp100`	ramp	30	100	20	330	25.86
`collision2D_h20ramp150`	ramp	30	150	20	337	26.23
`collision2D_h20ramp200`	ramp	30	200	20	345	26.43
`collision2D_h0ramp50`	ramp	20	50	0	323	25.82
`collision2D_h0ramp100`	ramp	20	100	0	367	26.23
`collision2D_h0ramp150`	ramp	20	150	0	348	32.49
`collision2D_h0ramp200`	ramp	20	200	0	313	37.01
`collision2D_upper_plate`	ramp	20	70	0	242	22.72
`collision2D_lower_plate`	cosine	20	150	0	381	26.46
`collision2D_flemish_cap`	ramp	21	70	12	403	27.73
`collision2D_grand_banks`	ramp	24	40	18	367	27.53
`collision2D_galicia_bank`	double ramp	16	70	10	-	-
`collision2D_siap`	ramp	22	80	14	385	27.63

collision2D_more	ramp	25	50	20	359	27.67
collision2D_jameson_liverpool	sine + cosine	22	160	14	396	27.68
collision2D_esperito_santo	ramp	25	70	20	368	27.68
collision2D_angola	double ramp	22.5	130	15	337	42.83

Table A.2: List of all the models with a ramp-type geometry. We also report here the models representing the real margins on Earth, which in some cases present coplicated geometries.

Adding an oceanic crust				
Model name	**Average ocean thickness** (km)	**Initial Ocean thickness** (km)	**Break-off depth** (km)	**Break-off time** (Myr)
collision2D_more	0	0	359	27.26
collision2D_eclogite20	20	20	348	25.06
collision2D_more_eclogite	7	7	356	27.12
collision2D_more_slab_b2e	7	7	374	22.47
collision2D_more_slab_b2e20	20	20	363	24.52
collision2D_more_b2e	13.5	20	348	22.21

Table A.3: This table reports the models in which we experimented with adding an oceanic crust. The first model does not include the oceanic crust. In the initial setup of the following two, the oceanic crust has not reached the trench yet, whilw in the last two the oceanic crust is already part of the slab.

First rheology models					
Model name	**Average continent thickness** (km)	**Average ocean thickness** (km)	**Margin viscosity** (Pa s)	**Break-off depth** (km)	**Break-off time** (Myr)
`rheology_MP01_odg`	25	13.5	10^{22}	351	15.27
`rheology_MP015_odg`	25	13.5	5×10^{22}	330	14.95
`rheology_MPm01_odg`	25	13.5	10^{21}	381	22.79
`rheology_MPm015_odg`	25	13.5	5×10^{21}	351	18.53

Table A.4: In this models we started to introduce some variations in the viscosiy of the margin, while maintaining a ramp-type geometry.

Magma poor margins					
Model name	**Margin length** (km)	**Viscosity** (Pa s)	**Break-off depth** (km)	**Break-off time** (Myr)	**Accreted margin material** (%)
`rheology_ramp100`	100	10^{23}	309	32.16	20
`rheology_ramp200`	200	10^{23}	309	34.06	50
`rheology_ramp300`	300	10^{23}	289	42.64	60
`rheology_ramp400`	400	10^{23}	268	56.66	70
`rheology_ramp500`	500	10^{23}	278	62.26	80
`rheology_ramp100_1e21`	100	10^{21}	361	20.18	40
`rheology_ramp200_1e21`	200	10^{21}	413	24.73	50
`rheology_ramp300_1e21`	300	10^{21}	392	37.98	50

rheology_ ramp400_ 1e21	400	10^{21}	433	41.53	60
rheology_ ramp500_ 1e21	500	10^{21}	443	46.6	60
rheology_ ramp100_ 1e22	100	10^{22}	351	35.96	30
rheology_ ramp200_ 1e22	200	10^{22}	330	43.26	40
rheology_ ramp300_ 1e22	300	10^{22}	320	50.80	55
rheology_ ramp400_ 1e22	400	10^{22}	330	57.69	50
rheology_ ramp500_ 1e22	500	10^{22}	309	65.14	45
rheology_ ramp300_ 5e20	300	5×10^{20}	289	33.89	40
rheology_ ramp300_ 5e21	300	5×10^{21}	412	41.77	50
rheology_ ramp300_ 5e22	300	5×10^{22}	351	24.95	45

Table A.5: Complete list of the magma poor margins. The comparison between all of these models can be found in figure 4.7.

Magma rich margins					
Model name	**Margin geometry**	**Margin length** (km)	$\Delta\rho_{pm}$ (kg/m^3)	**Break-off depth** (km)	**Break-off time** (Myr)
`rheology_ramp50_1e24`	ramp	50	500	322	16.61
`rheology_ramp100_1e24`	ramp	100	500	330	15.94
`rheology_ramp50_dr0`	ramp	50	0	330	20.04
`rheology_ramp100_dr0`	ramp	100	0	310	16.62
`rheology_ramp50_dr100`	ramp	50	-100	320	19.135
`rheology_ramp100_dr100`	ramp	100	-100	330	17.17
`rheology_ramp50_dr200`	ramp	50	-200	371	17.62
`rheology_ramp100_dr200`	ramp	100	-200	361	17.64
`ocean_ramp50_1e24`	fig. 4.9a	50	500	278	18.51
`ocean_ramp100_1e24`	fig. 4.9a	100	500	268	18.08
`ocean_ramp50_dr0`	fig. 4.9a	50	0	309	18.05
`ocean_ramp100_dr0`	fig. 4.9a	100	0	289	18.54
`ocean_ramp50_dr100`	fig. 4.9a	50	-100	350	18.66

ocean_ramp100_dr100	fig. 4.9a	100	-100	300	18.38
ocean_ramp50_dr200	fig. 4.9a	50	-200	361	19.25
ocean_ramp100_dr200	fig. 4.9a	100	-200	320	18.51
big_HVZ_ramp50dr0	fig. 4.9b	50	0	320	42.49
big_HVZ_ramp100dr0	fig. 4.9b	100	0	371	44.57
big_HVZ_ramp50dr100	fig. 4.9b	50	-100	340	43.82
big_HVZ_ramp100dr100	fig. 4.9b	100	-100	392	43.73
big_HVZ_ramp50dr200	fig. 4.9b	50	-200	330	43.21
big_HVZ_ramp100dr200	fig. 4.9b	100	-200	423	40.42
rheology_HVZ_ramp50dr0	fig. 4.9c	50	0	351	43.11
rheology_HVZ_ramp100dr0	fig. 4.9c	100	0	330	44.25
rheology_HVZ_ramp50dr100	fig. 4.9c	50	-100	361	43.39
rheology_HVZ_ramp100dr100	fig. 4.9c	100	-100	351	43.79
rheology_HVZ_ramp50dr200	fig. 4.9c	50	-200	340	43.69
rheology_HVZ_ramp100dr200	fig. 4.9c	100	-200	433	63.32

HVZ_ step50dr0	fig. 4.9d	50	0	278	43.43
HVZ_ step50dr0	fig. 4.9d	100	0	382	38.76
HVZ_ step50dr0	fig. 4.9d	50	-100	289	44.57
HVZ_ step50dr0	fig. 4.9d	100	-100	258	45.65
HVZ_ step50dr0	fig. 4.9d	50	-200	258	39.21
HVZ_ step50dr0	fig. 4.9d	100	-200	248	44.2

Table A.6: This table presents all the magma rich models. The first eight models outlined here represent the first step towards describing the more complicated geometries shown in figure 4.9, and represents a ramp-type margin with a fixed value of the viscosity and without oceanic crust.

Appendix B

Accreted material

In this appendix I present the figures I obtained when plotting the margin material that remains in the first 40 km of the domain throughout the computation, as a function of all the viscosities and margin length included in this study for magma poor margins.

The interest in analyzing this feature arises from the fact that traces of margin material can be found in orogenic belts in nature. The numerical values of the percentages of the accreted margin material shown in the figures below can be found in table A.5 in appendix A.

B.1 Accreted material as a function of length

The figures below show the percentage of margin material that subducts, exhumes or accretes on the overriding plate, as a function of the margin length. The dots represent the time of slab break-off. The specifics of the models can be found in appendix A. The trend is similar for all the models: the margin material sinks into the mantle in the early stages of subduction, then the break-off occurs and part of it exhumes. The value of the material in the first 40 km of the domain at the end of computation is the percentage of accreted material on the overriding plate.

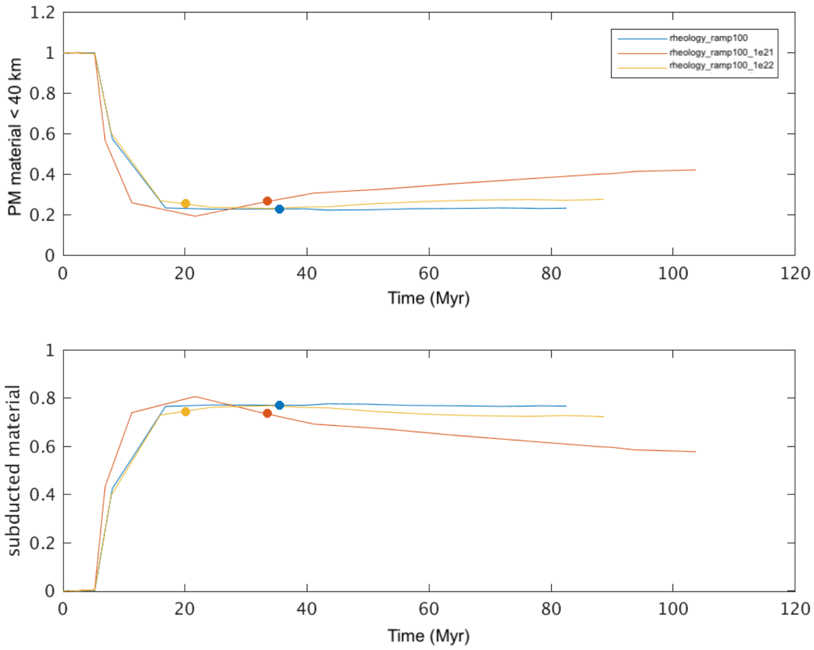

Figure B.1: Magma poor margin material which gets subducted and, eventually, accreted on the overriding plate for a margin of length 100 km and variable viscosity.

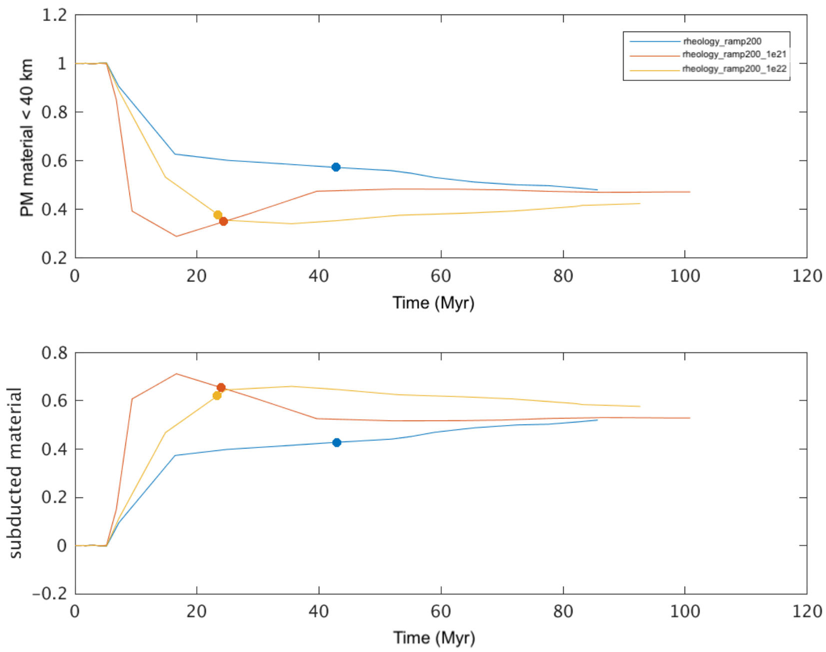

Figure B.2: Magma poor margin material which gets subducted and, eventually, accreted on the overriding plate for a margin of length 200 km and variable viscosity.

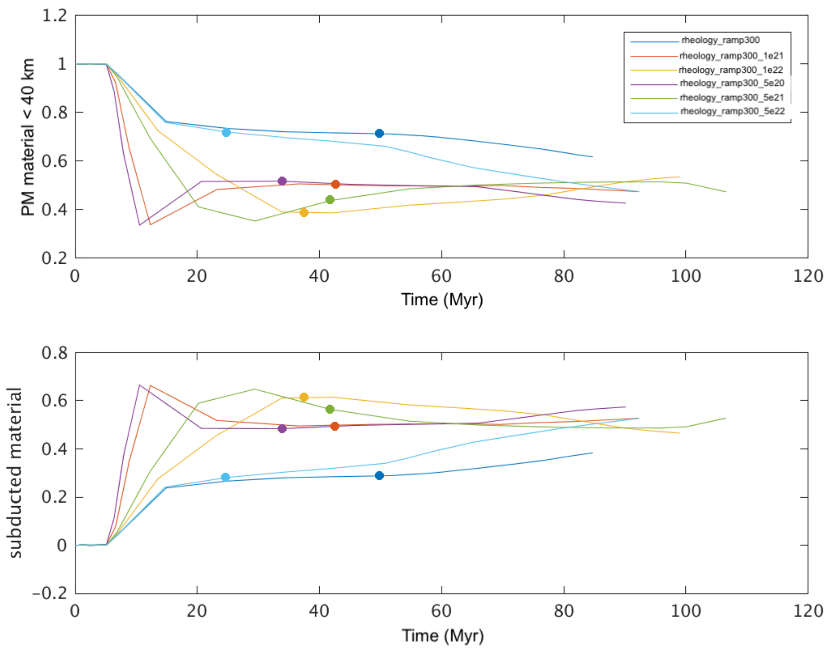

Figure B.3: Magma poor margin material which gets subducted and, eventually, accreted on the overriding plate for a margin of length 300 km and variable viscosity.

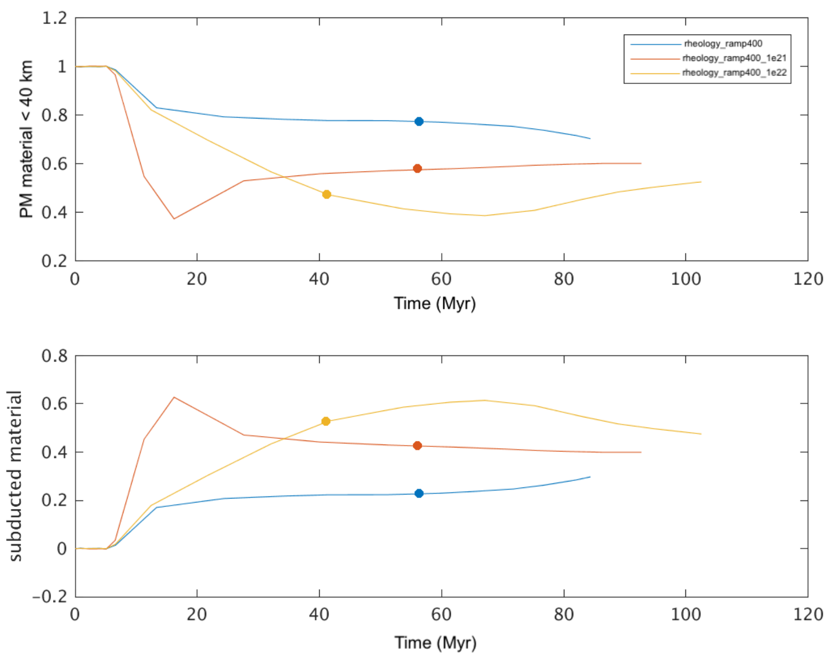

Figure B.4: Magma poor margin material which gets subducted and, eventually, accreted on the overriding plate for a margin of length 400 km and variable viscosity.

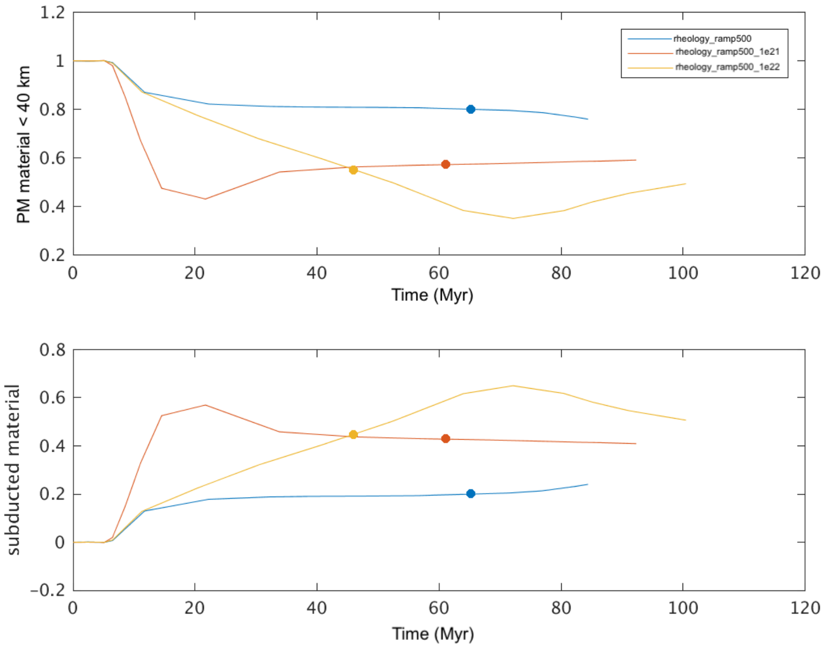

Figure B.5: Magma poor margin material which gets subducted and, eventually, accreted on the overriding plate for a margin of length 500 km and variable viscosity.

B.2 Accreted material as a function of viscosity

The figures below show the percentage of margin material that subducts, exhumes or accretes on the overriding plate, as a function of the margin viscosity. The dots represent the time of slab break-off. The specifics of the models can be found in appendix A. The trend is similar for all the models: the margin material sinks into the mantle in the early stages of subduction, then the break-off occurs and part of it exhumes. We can notice that, in general, when the ramp is short there is less accreted material at the end of computation. The value of the material in the first 40 km of the domain at the end of computation is the percentage of accreted material on the overriding plate.

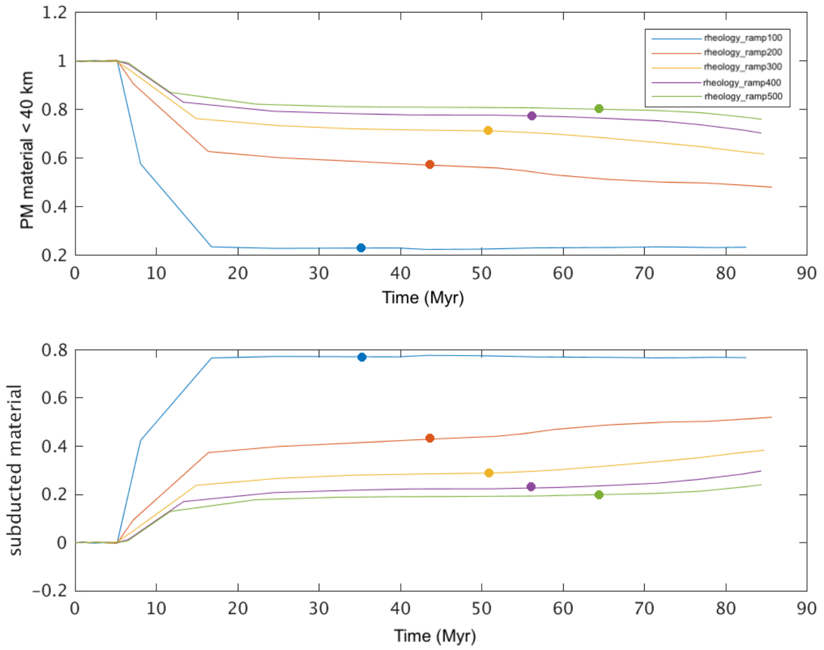

Figure B.6: Magma poor margin material which gets subducted and, eventually, accreted on the overriding plate for a margin of viscosity 10^{23}Pa s and variable length.

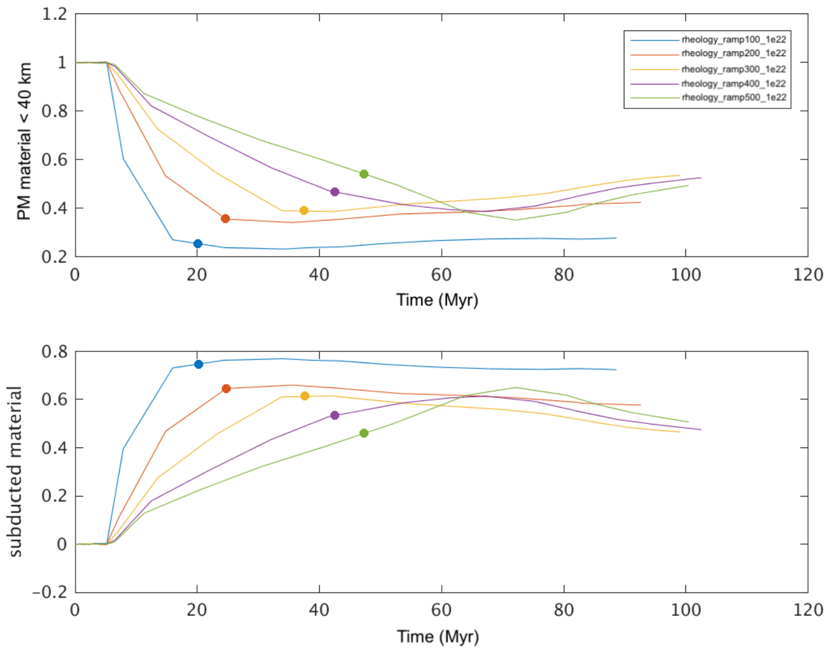

Figure B.8: Magma poor margin material which gets subducted and, eventually, accreted on the overriding plate for a margin of viscosity 10^{22}Pa s and variable length.

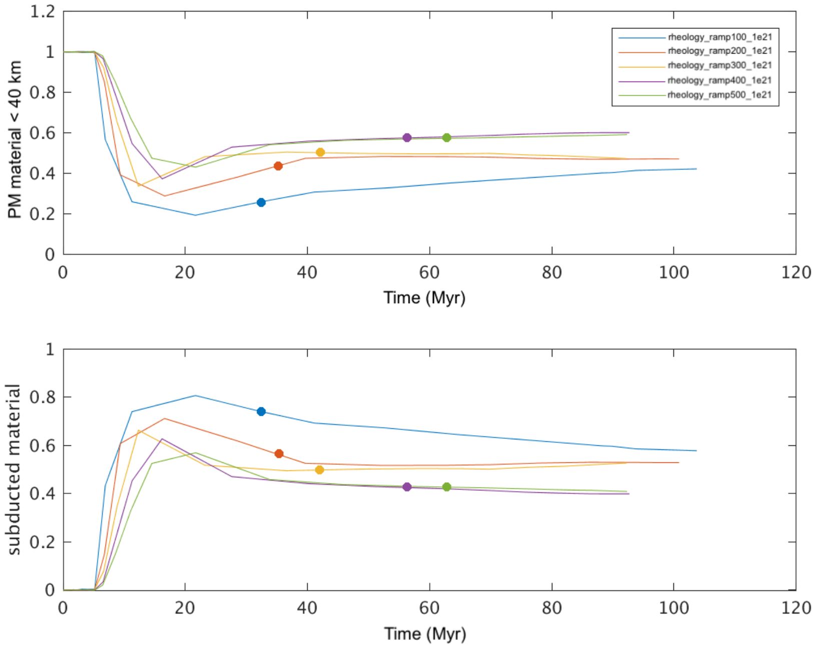

Figure B.7: Magma poor margin material which gets subducted and, eventually, accreted on the overriding plate for a margin of viscosity 10^{21}Pa s and variable length.

Bibliography

[1] D. Turcotte and G. Schubert, *Geodynamics*. Cambridge university press, 2014.

[2] D. P. McKenzie, “Speculations on the consequences and causes of plate motions,” *Geophysical Journal International*, vol. 18, no. 1, pp. 1–32, 1969.

[3] M. Cloos, “Lithospheric buoyancy and collisional orogenesis: Subduction of oceanic plateaus, continental margins, island arcs, spreading ridges, and seamounts,” *Geological Society of America Bulletin*, vol. 105, no. 6, pp. 715–737, 1993.

[4] S. Leyva, “Transform fault boundaries triple junctions.”

[5] V. v. Magni, J. Van Hunen, F. Funiciello, and C. Faccenna, “Numerical models of slab migration in continental collision zones.,” *Solid earth.*, vol. 3, no. 2, pp. 293–306, 2012.

[6] G. Péron-Pinvidic and G. Manatschal, “The final rifting evolution at deep magma-poor passive margins from iberia-newfoundland: a new point of view,” *International Journal of Earth Sciences*, vol. 98, no. 7, pp. 1581–1597, 2009.

[7] J. van Hunen and M. B. Allen, “Continental collision and slab break-off: a comparison of 3-d numerical models with observations,” *Earth and Planetary Science Letters*, vol. 302, no. 1-2, pp. 27–37, 2011.

[8] C. Baumann, T. V. Gerya, and J. A. Connolly, “Numerical modelling of spontaneous slab breakoff dynamics during continental collision,” *Geological Society, London, Special Publications*, vol. 332, no. 1, pp. 99–114, 2010.

[9] G. Toussaint, E. Burov, and L. Jolivet, “Continental plate collision: Unstable vs. stable slab dynamics,” *Geology*, vol. 32, no. 1, pp. 33–36, 2004.

[10] S. E. Williams, J. M. Whittaker, J. A. Halpin, and R. D. Müller, “Australian-antarctic breakup and seafloor spreading: Balancing geological and geophysical constraints,” *Earth-Science Reviews*, vol. 188, pp. 41–58, 2019.

[11] D. Franke, “Rifting, lithosphere breakup and volcanism: Comparison of magma-poor and volcanic rifted margins,” *Marine and Petroleum geology*, vol. 43, pp. 63–87, 2013.

[12] G. Manatschal, L. Lavier, and P. Chenin, “The role of inheritance in structuring hyperextended rift systems: Some considerations based on observations and numerical modeling,” *Gondwana Research*, vol. 27, no. 1, pp. 140–164, 2015.

[13] G. Mohn, G. Manatschal, M. Beltrando, and I. Haupert, “The role of rift-inherited hyper-extension in alpine-type orogens,” *Terra Nova*, vol. 26, no. 5, pp. 347–353, 2014.

[14] L. Geoffroy, “Volcanic passive margins,” *Comptes Rendus Geoscience*, vol. 337, no. 16, pp. 1395–1408, 2005.

[15] J.-P. Callot, L. Geoffroy, and J.-P. Brun, “Development of volcanic passive margins: Three-dimensional laboratory models,” *Tectonics*, vol. 21, no. 6, pp. 2–1, 2002.

[16] R. Whitmarsh, G. Manatschal, and T. Minshull, “Evolution of magma-poor continental margins from rifting to seafloor spreading,” *Nature*, vol. 413, no. 6852, pp. 150–154, 2001.

[17] E. Garzanti, C. Doglioni, G. Vezzoli, and S. Ando, “Orogenic belts and orogenic sediment provenance,” *The Journal of Geology*, vol. 115, no. 3, pp. 315–334, 2007.

[18] G. Manatschal, “New models for evolution of magma-poor rifted margins based on a review of data and concepts from west iberia and the alps,” *International Journal of Earth Sciences*, vol. 93, pp. 432–466, 06 2004.

[19] G. Peron-Pinvidic, G. Manatschal, and P. T. Osmundsen, “Structural comparison of archetypal atlantic rifted margins: A review of observations and concepts,” *Marine and Petroleum Geology*, vol. 43, pp. 21 – 47, 2013.

[20] I. Haupert, G. Manatschal, A. Decarlis, and P. Unternehr, “Upper-plate magma-poor rifted margins: Stratigraphic architecture and structural evolution,” *Marine and Petroleum Geology*, vol. 69, pp. 241–261, 2016.

[21] L.-N. Moresi and V. Solomatov, “Numerical investigation of 2d convection with extremely large viscosity variations,” *Physics of Fluids*, vol. 7, no. 9, pp. 2154–2162, 1995.

[22] S. Zhong, M. T. Zuber, L. Moresi, and M. Gurnis, "Role of temperature-dependent viscosity and surface plates in spherical shell models of mantle convection," *Journal of Geophysical Research: Solid Earth*, vol. 105, no. B5, pp. 11063–11082, 2000.

[23] C.-C. Yu and J. C. Heinrich, "Petrov—galerkin method for multidimensional, time-dependent, convective-diffusion equations," *International Journal for numerical methods in engineering*, vol. 24, no. 11, pp. 2201–2215, 1987.

[24] E. Di Giuseppe, J. Van Hunen, F. Funiciello, C. Faccenna, and D. Giardini, "Slab stiffness control of trench motion: Insights from numerical models," *Geochemistry, Geophysics, Geosystems*, vol. 9, no. 2, 2008.

[25] J. van Hunen, A. P. Van Den BERG, and N. J. Vlaar, "On the role of subducting oceanic plateaus in the development of shallow flat subduction," *Tectonophysics*, vol. 352, no. 3-4, pp. 317–333, 2002.

[26] G. Ranalli, "Rheology of the crust and its role in tectonic reactivation," *Journal of geodynamics*, vol. 30, no. 1-2, pp. 3–15, 2000.

[27] S.-i. Karato and P. Wu, "Rheology of the upper mantle: A synthesis," *Science*, vol. 260, no. 5109, pp. 771–778, 1993.

[28] K. Lambeck and P. Johnston, *The viscosity of the mantle: evidence from analyses of glacial rebound phenomena*. Cambridge University Press, Cambridge, 1998.

[29] D. Kohlstedt, B. Evans, and S. Mackwell, "Strength of the lithosphere: Constraints imposed by laboratory experiments," *Journal of Geophysical Research: Solid Earth*, vol. 100, no. B9, pp. 17587–17602, 1995.

[30] J. Byerlee, "Friction of rocks," in *Rock friction and earthquake prediction*, pp. 615–626, Springer, 1978.

[31] M. I. Billen and M. Gurnis, "A low viscosity wedge in subduction zones," *Earth and Planetary Science Letters*, vol. 193, no. 1-2, pp. 227–236, 2001.

[32] M. Stab, N. Bellahsen, R. Pik, X. Quidelleur, D. Ayalew, and S. Leroy, "Modes of rifting in magma-rich settings: Tectono-magmatic evolution of central afar," *Tectonics*, vol. 35, no. 1, pp. 2–38, 2016.

[33] B. R. Hacker *et al.*, "Eclogite formation and the rheology, buoyancy, seismicity, and h˜ 2o content of oceanic crust," *GEOPHYSICAL MONOGRAPH-AMERICAN GEOPHYSICAL UNION*, vol. 96, pp. 337–346, 1996.

[34] J. Jakob, T. B. Andersen, and H. J. Kjøll, "A review and reinterpretation of the architecture of the south and south-central scandinavian caledonides—a magma-poor to magma-rich transition and the significance of the reactivation of rift inherited structures," *Earth-science reviews*, 2019.

Acknowledgements

First of all, I want to thank Professor Andrea Morelli and Valentina, without whom this thesis would not have existed.

Professor Morelli, thank you for helping me to find this opportunity and for the feedback you gave me throughout the entire work. I am really thankful for all your help and suggestions.

Valentina, thank you for teaching me all the tools I learnt to use for this thesis, as well as for sharing with me all your knowledge on Geology and making me understand how to approach the kind of problems I studied. I also want to thank you for helping me feel at home in Oslo, thanks to you I never felt out of place and I'm really glad I was able to work with you.

A huge thank you goes to my family. Mom, dad, Simo and Michi: without your help and support I would not be able to pursue my goals, even when it comes to my studies. Thank you for encouraging me to follow my dreams, always. A special thank you to my nephews, Samu and Tommy. Without all the hours I spent playing with you, I would have certainly gone crazy while writing this thesis.

I also want to thank all of the people I met at CEED. Thank you for making me feel welcome and helping me with this project. In particular, I want to thank my office mates, Rebecca, Petra, Kristina, Helge and Michael. Thank you for all the incredibly long coffee breaks: without you my life in Oslo would have certainly been duller (and probably a bit more productive).

Many thanks to all of my friends in Oslo, especially René, Kate and Anne Katherine. Thanks for listening to all of my ramblings about this thesis, and making fun of me because of it.

Last, but not least, I want to thank all of the important people who share their lives with me in Milan and Bologna: Marco, Fede, Linda, Corrado, Ste, Cami, Carlo, Chiara, Luca, Lore and Letizia. Thank you for constantly supporting me though this master and always making me feel part of your lives, even when I was 2000 km away.

To all of you I dedicate this thesis.